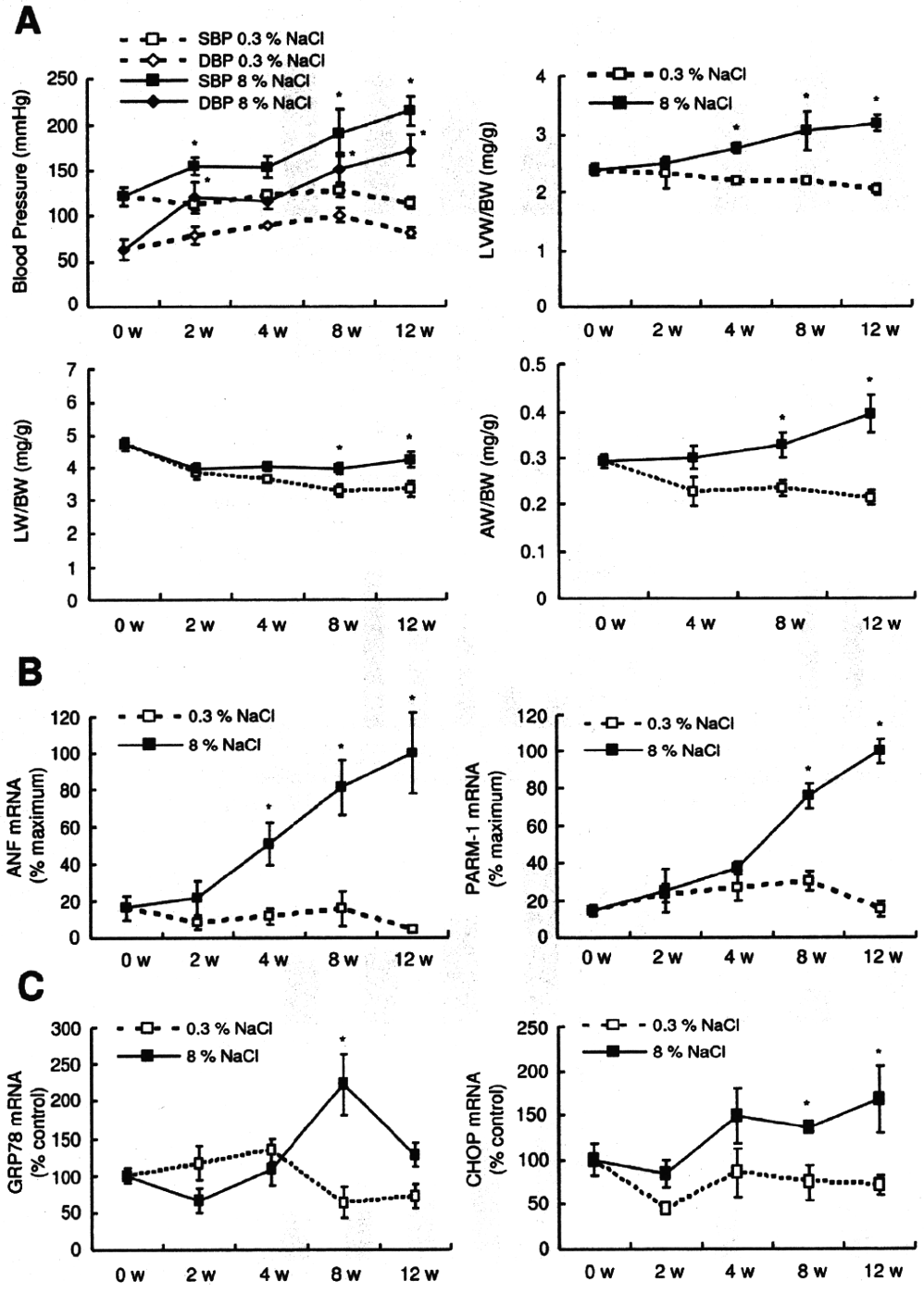

Figure 2. PARM-1 expression and ER stress response was activated in hypertensive heart disease model of Dahl salt-sensitive rats. *A*: The animals were subjected to a high- (8% NaCl, n = 12 for each time point) or low-salt diet (0.3% NaCl, n = 8 for each time point). Blood pressure and left ventricular weight (LVW), Body weight (BW), lung weight (LW) and atrial weight (AW) were measured at the indicated periods of time after starting the designated diet. *B, C*: ANF and PARM-1 expression (B), and ER stress markers such as GRP78 and CHOP (C) were analyzed by kinetic real-time PCR on cDNAs from the hearts of Dahl salt-sensitive rats. *$P<0.05$ versus a low-salt diet group at the respective time point.
doi:10.1371/journal.pone.0009746.g002

PARM-1 does not induce programmed cell death [8]. Although ectopic expression of human PARM-1 in a prostate cancer cell line results in increased colony formation [15], suggesting a probable role of PARM-1 in cell proliferation, the others reported that transient expression of rat PARM-1 does not alter the proliferative property of another prostate cancer cell line [16]. Thus, the

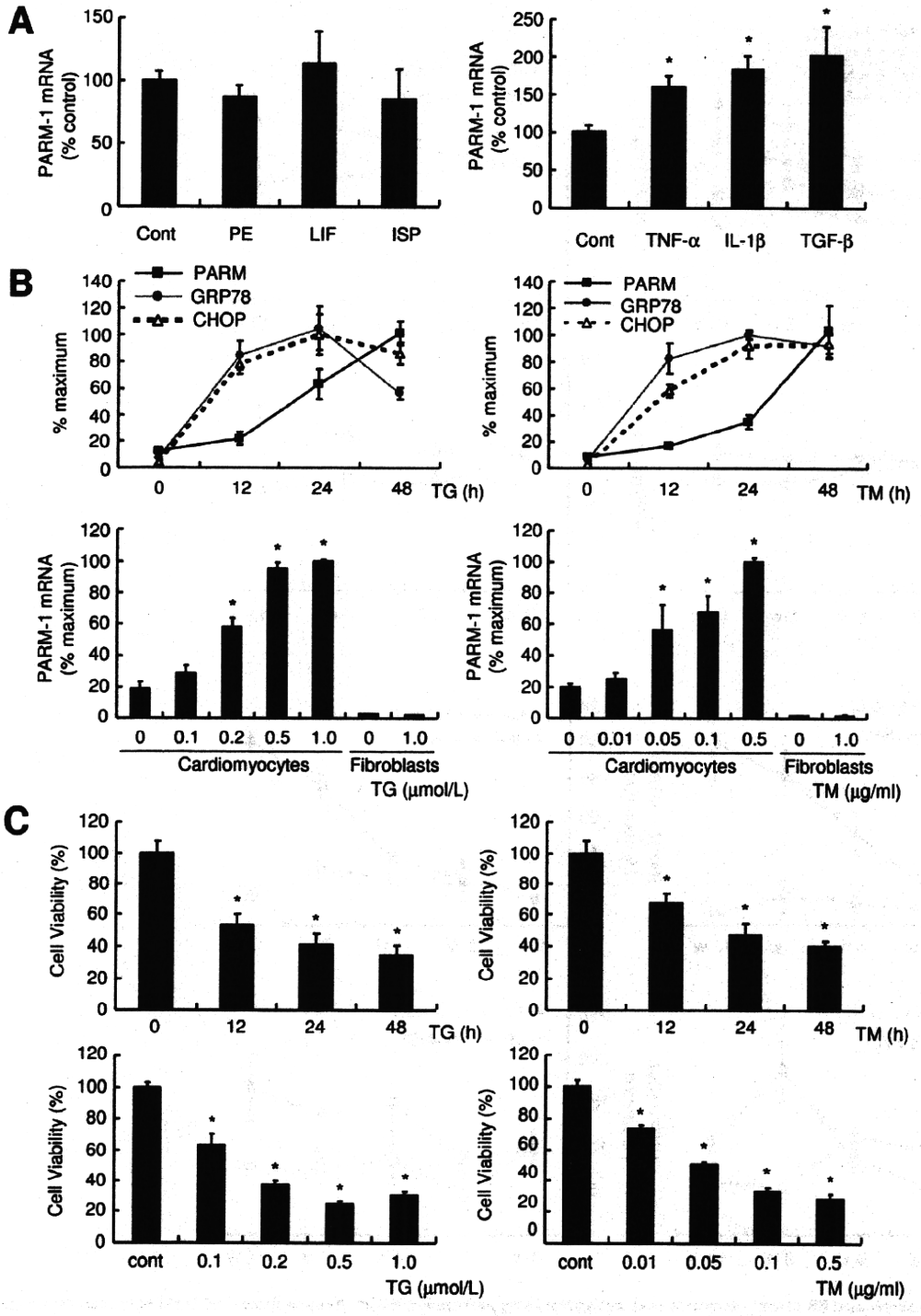

Figure 3. PARM-1 expression was induced by inflammatory cytokines and ER stress inducers specifically in cardiac myocytes. *A*: Cultured rat neonatal cardiac myocytes were stimulated by hypertrophic stimuli such as 100 μmol/l phenylephrine (PE), 1000 U/ml leukemia inhibitory factor (LIF) and 10 μmol/l isoproterenol (ISP), or inflammatory cytokines such as 100 ng/ml TNF-α, 5 ng/ml IL-1β and 4 ng/ml TGF-β. PARM-1 expression was analyzed 48 hours after stimulation. *B*: Cardiac myocytes were treated with 0.5 μmol/l thapsigargin (TG) or 0.1 μg/ml tunicamycin (TM) for the indicated periods of time, and GRP78, CHOP and PARM-1 expression was analyzed by kinetic real time PCR. *C*: Cardiac myocytes and fibroblasts were treated with TG or TM for 48 hours at the indicated concentration, and PARM-1 expression was analyzed. *D*: Cardiac myocytes were treated with TG or TM as indicated, and cell viability was assessed by WST-8 assay. *$P<0.05$ versus non-treated control cells.
doi:10.1371/journal.pone.0009746.g003

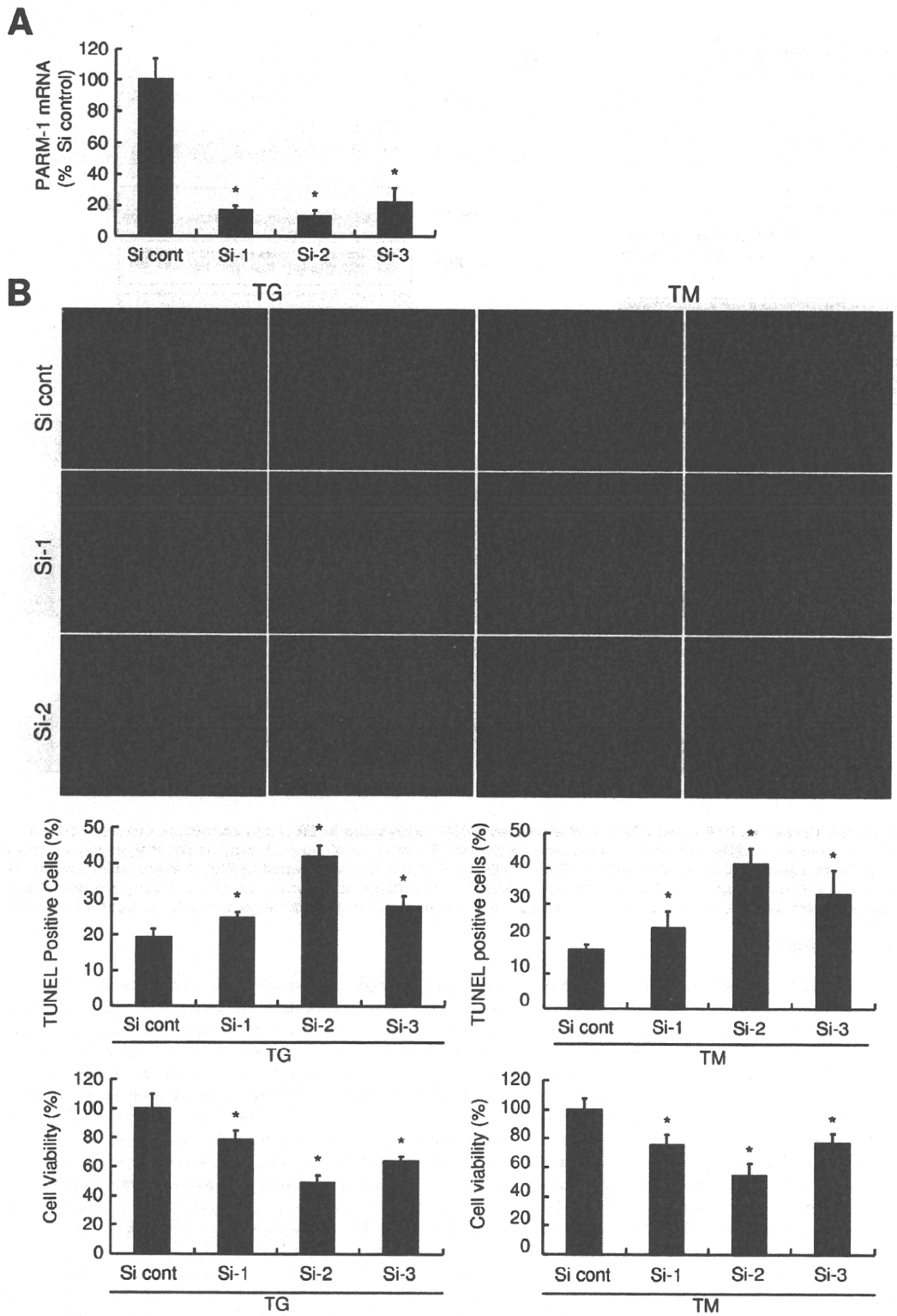

Figure 4. Silencing of PARM-1 augmented apoptotic response to ER stress. *A*: Cultured neonatal rat cardiac myocytes were transfected with 30 nmol/l of three different siRNA duplexes, and assessed for PARM-1 expression 24 hours after transfection. *B*: Cells were treated with TG or TM 72 hours after transfection with siRNAs for 24 hours. Apoptotic cell death was assessed by TUNEL assay, and cell viability was analyzed by WST-8 assay. *$P<0.05$ versus control siRNA (Si cont).
doi:10.1371/journal.pone.0009746.g004

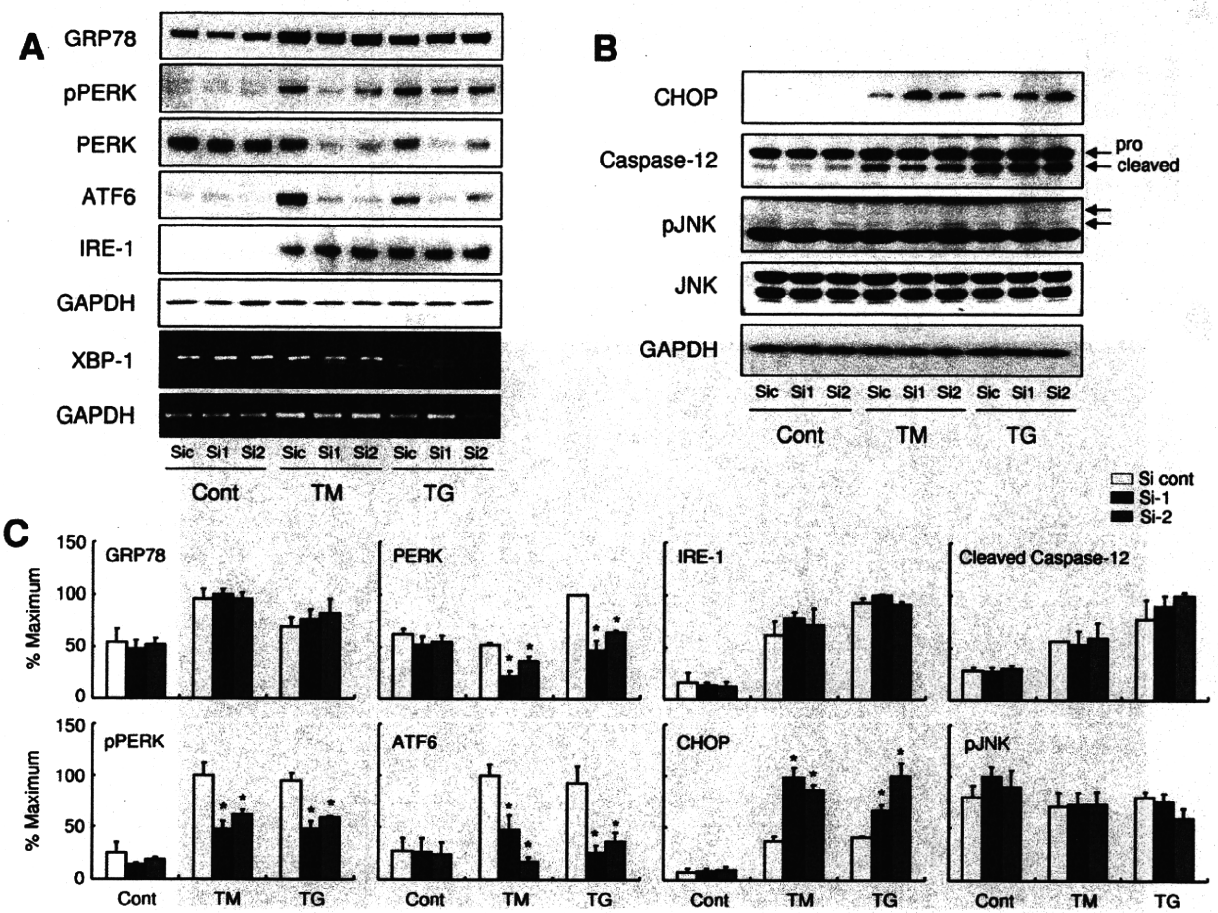

Figure 5. PARM-1 silencing decreases PERK and ATF6, and increases CHOP expression in ER stress condition. Cultured neonatal rat cardiac myocytes were transfected with siRNAs, and, after 72 hours, were treated with TM or TG for 48 hours. *A*: Immunoblot analysis was performed with antibody against GRP78, phospho-PERK, PERK, ATF6, IRE-1 or GAPDH. XBP-1 mRNA splicing was assessed by PCR. *B*: Immunoblot analysis was performed with antibody against CHOP, Caspase-12, phospho-JNK, JNK or GAPDH. *C*: Densitometric analysis was carried out using ImageJ software. The results were normalized against GAPDH, and expressed as percentages of the maximum. $^*P<0.05$ versus control siRNA (Si cont) of respective treatment with TM or TG.
doi:10.1371/journal.pone.0009746.g005

regulation of PARM-1 especially in other organs than prostate, and its roles are largely unknown.

Our analysis on hypertensive heart disease model of Dahl salt-sensitive rats demonstrated that PARM-1 expression was significantly upregulated following a high-salt diet. While one of the early cardiac manifestations of this model is hypertension-induced cardiac hypertrophy [10,11], PARM-1 expression was unchanged 4 weeks after starting a high-salt diet, when a significant increase in LVW to BW ratio was already detected (Fig. 2A,B). Further, in cultured cardiac myocytes, stimulation with hypertrophic stimuli did not alter the expression of PARM-1 (Fig. 3A). This could be in accordance with PARM-1 expression in the hearts during normal developmental stages. While a common feature of various hypertrophic responses is re-activation of fetal gene programs such as ANF and skeletal α-actin genes [17], PARM-1 expression readily detectable at E10.5 was increased toward neonatal stages, and then maintained through adult stages (Fig. 1C). These results suggested that PARM-1 expression could not be a part of fetal gene programs or hypertrophic responses. Another feature of hypertensive heart disease is a development of heart failure. In our model, 8 weeks after staring a high-salt diet, a significant increase in LW to BW ratio was observed, indicating the presence of lung congestion. Although we did not detected a significant increase in LV dimension and a decrease in fractional shortening up to 12 weeks of a high-salt diet (data not shown), a significant increase in AW to BW ratio was noted at 8 weeks, suggesting the development of diastolic heart failure in this model. In this model, PARM-1 was significantly upregulated 8 weeks after starting a high-salt diet, suggesting that PARM-1 was induced in the setting of heart failure. Development of heart failure involves neurohumoral and inflammatory mechanisms [18,19], and recent evidences have suggested that ER stress plays an important role in the pathogenesis of heart failure [12,13]. In cultured cardiac myocytes, inflammatory cytokines stimulated PARM-1 expression (Fig. 3A). Further, ER stress inducers, thapsigargin and tunicamycin markedly upregulated PARM-1 expression (Fig. 3B), and ER stress markers such as GRP78 and CHOP were also upregulated in the hearts of hypertensive heart disease model at the heart failure phase (Fig. 2C). These results implied that PARM-1 expression is upregulated during heart failure, involving inflammatory cytokines and ER stress.

As PARM-1 was localized in ER in cardiac myocytes, and ER stress induced PARM-1 expression, PARM-1 could play a role in ER stress response. ER is a cellular organelle, where protein synthesis and folding of secreted and transmembrane proteins take place. When ER environment is perturbed, and the folding of nascent proteins is impaired, a quality control system called UPR is activated [12,13,14]. Initially, UPR is an adaptive response in which the cells attempt to overcome the accumulation of misfolded proteins through augmenting protein folding capacity. However, when ER stress is excessive and prolonged, cells undergo apoptotic cell death. Thus, ER stress response has a conditional ability to protect the cells or activate cell death program. In the hearts, ER stress response has been shown to be activated in several pathological models including myocardial infarction, ischemia/reperfusion and pressure overload-induced hypertrophy [20,21,13,22]. Pressure overload by transverse aortic constriction has been shown to induce prolonged ER stress during the transition from cardiac hypertrophy to heart failure [20]. AMP-activated protein kinase protects cardiac myocytes from hypoxic injury by attenuating ER stress [23]. Aberrant ER quality control in transgenic mice with mutant KDEL receptor, or chronic myocardial inflammation induced by chemoattractant protein-1 transgene activates ER stress response and causes heart failure [24,25]. These results indicated that ER stress response could be deleterious in the hearts. In contrast, overexpression of ER stress gene GRP94 protects cardiac myocytes from oxidative injury [26], and inducible transgene of activated form of ATF6 in the hearts protects the hearts from ischemia/reperfusion damage [27], suggesting the protective role of ER stress response in the hearts. Thus, the outcome of ER stress response is also context dependent in the heart. In our model of hypertensive heart disease, ER stress response assessed by the expression of GRP78 and CHOP was activated in the phase of transition from hypertrophy to heart failure (Fig. 2C). While GRP78 expression reached a peak at 8 weeks of diet and then declined, CHOP expression remained upregulated until 12 weeks. Those expression patterns might be compatible with those reported in transverse aortic constriction-induced heart failure model, as a peak expression of GRP78 is observed at 1 week after transverse aortic constriction, while CHOP is upregulated even at 4 weeks [20]. Since induction of ER chaperone GRP78 represents a major survival arm of ER stress response, and indeed, overexpression of ER chaperone is protective for cardiac myocytes from ischemia and calcium overload injuries [26], these observations could be in good accordance with the general view that the UPR has a protective role during initial phase of ER stress, while proapoptotic pathways are activated upon continued ER stress [12,13,14]. Thus, ER stress response in our model might have the deleterious effect in the transition to heart failure, while it is still possible that this ER stress response was a part of counteracting efforts against developing heart failure.

Consistent with the contradictory roles of ER stress response in cell survival and death, ER stress has been demonstrated to activate both prosurvival and apoptotic signaling pathways [13,14]. In cultured cardiac myocytes, treatment of cardiac myocytes with ER stress inducers resulted in reduced viability and increased apoptotic cell death [20]. In this setting, PARM-1 expression was markedly increased (Fig. 3B), and silencing PARM-1 expression significantly augmented ER stress-induced cell death (Fig. 4B), indicating PARM-1 is a part of cell survival pathways in ER stress response. Given that PARM-1 expression was induced in the phase of transition to heart failure in hypertensive heart disease model of Dahl salt-sensitive rats (Fig. 2B), the increased expression of PARM-1 in this model could play a role to counteract against development of heart failure through inhibiting apoptosis of cardiac myocytes, although further studies are needed to determine the role of PARM-1 induction in the development of heart failure in vivo.

ER stress is sensed by three distinct ER sensory proteins, PERK, ATF6 and IRE-1, which are kept inactivated by binding with ER-resident chaperones such as GRP78 and GRP94. Upon accumulation of misfolded proteins in ER, the chaperones are occupied by misfolded proteins, which results in the release and activation of the ER stress sensors, and subsequent activation of downstream signaling pathways [12,13,14]. The downstream signaling effectors include prosurvival and proapoptotic pathways, and it is anticipated that the balance between prosurvival and proapoptotic pathways determines the ultimate outcome of ER stress response, while the precise molecular mechanisms involved in cell fate determination remain to be delineated. In this study, silencing of PARM-1 did not alter the expression of GRP78, suggesting the expression of PARM-1 was not involved in the regulation of ER stress itself, or expression of ER chaperones (Fig. 5A). Downregulation of PARM-1 expression by siRNA markedly attenuated the expression of PERK and ATF6 without affecting IRE1 induction and XBP-1 splicing. Interestingly, these effects of PARM-1 silencing on PERK and ATF6 expression were only observed upon stimulation with thapsigargin or tunicamycin (Fig. 5). These results suggested that PARM-1 plays a crucial role in maintaining PERK and ATF6 expression in the setting of ER stress conditions. Since overall PERK signaling is protective against cell death in most circumstances [13,14,28], and preactivation of ATF6 protects the heart against ischemia/reperfusion insult [27], maintenance of PERK and ATF6 expression by PARM-1 is critical for cardiac myocytes to cope with ER stresses. The CHOP, JNK and Caspases are distal effectors of ER stress response that have been implicated in mediating apoptotic signals. CHOP induction was markedly augmented by PARM-1 silencing, while activation of JNK and Caspase-12 was unaffected (Fig. 5B,C), indicating that PARM-1 was also mediating prosurvival effect by suppressing CHOP-mediated apoptotic pathways in cardiac myocytes. Expression of CHOP, but not activation of JNK and Caspase-12 has been shown to be induced by transverse aortic constriction in murine hearts [20]. In cultured cardiac myocytes, proteasome inhibitors are shown to activate ER stress response and apoptosis, in which silencing CHOP, but not inhibition of JNK or Caspase-12 rescues cardiac myocytes from apoptosis [29]. Thus, CHOP expression might be one of important mechanisms inducing cardiac myocyte apoptosis in response to ER stress, and PARM-1 has an inhibitory role in this pathway. As CHOP is known to be regulated downstream of PERK and ATF-6 [30,13,28], and PARM-1 is involved in the maintenance of PERK and ATF-6 without affecting IRE-1 induction and XBP-1 splicing, it looks likely that PARM-1 is involved in a specific set of signal transduction pathways in ER stress response, while further studies are clearly needed to delineate the molecular mechanisms by which PARM-1 regulates ER stress response pathways.

An intriguing finding of this study was PARM-1 expression and induction of PARM-1 by ER stress was specific for cardiac myocytes (Fig. 3B). Recently, several ER membrane molecules specific for certain cell types have been identified. Those include CREB4, CREB-H, Luman and OASIS, and are involved in ER stress response [31,32,33,34]. For example, CREB-H is expressed exclusively in the liver [35], and activated by ER stress [34]. However, ER stress-induced activation of CREB-H leads to induction of acute phase response genes such as C-reactive protein and serum amyloid P-component rather than canonical unfolded

protein responses [34]. Thus, ER stress response could have specialized roles in specialized cells. Although there is a striking difference between those molecules and PARM-1, as those belong to basic-leucine zipper transcription factor, and PARM-1 does not have any known domain for transcription factors, PARM-1 could mediate ER stress response specific for cardiac myocytes.

In this study, we identified PARM-1 as an ER protein specifically expressed in cardiac myocytes, and found that PARM-1 expression was induced in hypertensive heart disease model, and by ER stress in cardiac myocytes. Further, it was also shown that PARM-1 had a protective role against ER stress-induced apoptotic response in cardiac myocytes. As elucidation of cardiac specific ER stress response could have therapeutic impacts on many heart diseases, identification of molecular mechanisms regulated by PARM-1 will be an important issue to understand cardiac specific ER stress responses.

Materials and Methods

Cardiac myocytes culture

Neonatal rat cardiac myocytes and non-myocytes were prepared from 1-day-old Wistar rat hearts as described previously [36,37]. Neonatal rat ventricles were enzymatically digested, and cardiac myocytes were purified over a discontinuous Percoll gradient. Cardiac myocytes were cultured in DMEM/F-12 medium supplemented with 5% fetal bovine serum and 100 μmol/l 5-bromo-2-deoxyuridine (BrdU) for 16-24 hours, and culture medium was then changed to serum-deprived medium containing insulin, transferrin, selenium, bovine serum albumin and BrdU. Non-myocytes in the upper layer were plated onto non-coated culture dishes, and the attached cells were cultured and passaged. Non-myocytes at 2nd passage were used for the experiments. Each experiment was performed under serum free condition at least 24 hrs after serum deprivation.

Signal sequence trap

Signal sequence trap by retrovirus-mediated expression screening (SST-REX) was performed as previously described [6,9]. Briefly, a library was constructed in the retrovirus vector pMX-SST employing cDNA derived from poly(A)$^+$ RNA isolated from neonatal rat cardiac myocytes. The interleukin-3 (IL-3)-dependent pro-B cell line Ba/F3 [6,9] was infected with retrovirus, followed by seeding onto 96-multiwell plates in the absence of IL-3. Genomic DNA extracted from IL-3-independent Ba/F3 clones were subjected to PCR to recover the integrated cDNAs using primers specific for the cloning vector. After electrophoresis of the PCR products, DNA was recovered and subjected to sequencing.

Animals and treatments

Male Dahl salt-sensitive rats (6 weeks old) were purchased from Shimizu laboratory supplies. From 6 weeks onwards, these rats were fed a high-sodium diet (containing 8% NaCl) or a low-sodium diet (containing 0.3% NaCl) [10,11]. After 2, 4, 8 and 12 weeks, blood pressure was measured by the tail-cuff method. All procedures using animals performed in this study were approved by the Institutional Animal Care and Use Committee of Kyoto Prefectural University of Medicine.

Reverse transcriptase (RT)-PCR

Total RNA was extracted from rat tissues using TRIzol (Invitrogen) and from neonatal rat cardiac myocytes using the RNeasy mini kit (Qiagen), and then cDNA was synthesized by the High Capacity cDNA Reverse Transcription Kit (Applied Biosystems). Synthesized cDNA was analyzed by quantitative kinetic real-time PCR using the ABI Prism 7700 Sequence Detector system (Applied Biosystems) with SYBR Premix Ex Taq (Takara) [38,39]. Rat glyceraldehyde-3-phosphate dehydrogenase (GAPDH) was used for normalization, and the comparative threshold (C_T) method was used to assess the relative abundance of the targets. For XBP-1 mRNA splicing, the primers flanking the intron splicing site by IRE-1 was used for PCR, and the products were analyzed by agarose gel electrophoresis with visualization using ethidium bromide [40].

Immunostaining

Cells were stained with anti-flag M2 monoclonal antibody (Sigma) or goat polyclonal antibody against GRP78 (Santa Cruz), followed by Alexa Fluor 488- or Alexa Fluor 555-conjugated secondary antibody (Invitrogen). Mitochondria were stained with MitoTracker Green FM (Invitrogen) and nuclei were visualized using DAPI. Images were captured with a BZ-8000 microscope (Keyence).

Immunoblot analysis

Cells lysates normalized by protein concentration were subjected to 10% or 15% SDS-polyacrylamide gel electrophoresis, and transferred to polyvinylidene difluoride membranes (Millipore) [38,39]. Blots were immunoblotted with the primary antibody against GRP78, CHOP (Santa Cruz), phospho-PERK, PERK, IRE-1, phospho-JNK, JNK (Cell Signaling), Caspase-12 (Sigma) or ATF6 (AnaSpec), and horseradish peroxidase-labeled donkey secondary antibody, followed by enhanced chemiluminescence (GE Healthcare). Densitomeric analysis was performed using ImageJ software.

Small interfering RNA–mediated silencing

PARM-1 stealth siRNA duplexes were purchased from Invitrogen. Target sequences of siRNA are: siRNA-1; 5′-GAACACAGTCTCGGCAGTCCTGAAA-3′, siRNA-2; 5′-TCCGCTTCCGTTACCTCTAACCACA-3′, siRNA-3; 5′-GCGGCATATCTGAAGATCAGGCATT-3′. Cells were transfected with 30 nmol/L siRNA duplex using Lipofectamine RNAiMAX reagent (Invitrogen) according to the manufacture's instruction [41]. Stealth RNAi negative control (Invitrogen) was used as a control.

Cell viability and TUNEL assay

Cell viability was assessed using WST-8 (2-(2-methoxy-4-nitrophenyl)-3-(4-nitrophenyl)-5-(2,4-disulfophenyl)-2H-tetrazolium, monosodium salt) (Kishida Kagaku) according to the manufacturer's instruction. Apoptotic cells were detected by *in situ* terminal deoxynucleotidyl transferase-mediated biotinylated UTP nick end labeling (TUNEL) assay using ApopTag Red In Situ Apoptosis Detection Kit (Chemicon) as previously described [39]. Cells were nuclear stained with DAPI, and the TUNEL positive and total nuclei were counted under the fluorescent microscope (IX71, Olympus Corporation) in 5 view fields per well.

Statistical analysis

All experiments were performed at least three times in duplicates. Data were expressed as means ± standard errors and analyzed by unpaired Student's *t*-test for comparisons between two groups, or one-way ANOVA with post hoc analysis for multiple comparisons. A value of $p<0.05$ was considered statistically significant.

Acknowledgments

We thank M. Nakata and M. Kuramoto for expert technical assistance.

Author Contributions

Conceived and designed the experiments: KI TT TU HO HM. Performed the experiments: KI TT HI NN TO SA AA. Analyzed the data: KI TT HI NN. Wrote the paper: KI TT.

References

1. Jessup M, Brozena S (2003) Heart failure. N Engl J Med 348: 2007–2018.
2. Neubauer S (2007) The failing heart–an engine out of fuel. N Engl J Med 356: 1140–1151.
3. Fisher SA, Langille BL, Srivastava D (2000) Apoptosis during cardiovascular development. Circ Res 87: 856–864.
4. Dorn GW, 2nd (2009) Apoptotic and non-apoptotic programmed cardiomyocyte death in ventricular remodelling. Cardiovasc Res 81: 465–473.
5. Lee Y, Gustafsson AB (2009) Role of apoptosis in cardiovascular disease. Apoptosis 14: 536–548.
6. Kojima T, Kitamura T (1999) A signal sequence trap based on a constitutively active cytokine receptor. Nat Biotechnol 17: 487–490.
7. Tashiro K, Nakamura T, Honjo T (1999) The signal sequence trap method. Methods Enzymol 303: 479–495.
8. Bruyninx M, Hennuy B, Cornet A, Houssa P, Daukandt M, et al. (1999) A novel gene overexpressed in the prostate of castrated rats: hormonal regulation, relationship to apoptosis and to acquired prostatic cell androgen independence. Endocrinology 140: 4789–4799.
9. Ogata T, Ueyama T, Nomura T, Asada S, Tagawa M, et al. (2007) Osteopontin is a myosphere-derived secretory molecule that promotes angiogenic progenitor cell proliferation through the phosphoinositide 3-kinase/Akt pathway. Biochem Biophys Res Commun 359: 341–347.
10. Doi R, Masuyama T, Yamamoto K, Doi Y, Mano T, et al. (2000) Development of different phenotypes of hypertensive heart failure: systolic versus diastolic failure in Dahl salt-sensitive rats. J Hypertens 18: 111–120.
11. Klotz S, Hay I, Zhang G, Maurer M, Wang J, et al. (2006) Development of heart failure in chronic hypertensive Dahl rats: focus on heart failure with preserved ejection fraction. Hypertension 47: 901–911.
12. Wang X, Robbins J (2006) Heart failure and protein quality control. Circ Res 99: 1315–1328.
13. Glembotski CC (2007) Endoplasmic reticulum stress in the heart. Circ Res 101: 975–984.
14. Lai E, Teodoro T, Volchuk A (2007) Endoplasmic reticulum stress: signaling the unfolded protein response. Physiology (Bethesda) 22: 193–201.
15. Fladeby C, Gupta SN, Barois N, Lorenzo PI, Simpson JC, et al. (2008) Human PARM-1 is a novel mucin-like, androgen-regulated gene exhibiting proliferative effects in prostate cancer cells. Int J Cancer 122: 1229–1235.
16. Cornet AM, Hanon E, Reiter ER, Bruyninx M, Nguyen VH, et al. (2003) Prostatic androgen repressed message-1 (PARM-1) may play a role in prostatic cell immortalisation. Prostate 56: 220–230.
17. Barry SP, Davidson SM, Townsend PA (2008) Molecular regulation of cardiac hypertrophy. Int J Biochem Cell Biol 40: 2023–2039.
18. Blum A, Miller H (2001) Pathophysiological role of cytokines in congestive heart failure. Annu Rev Med 52: 15–27.
19. Conraads VM, Bosmans JM, Vrints CJ (2002) Chronic heart failure: an example of a systemic chronic inflammatory disease resulting in cachexia. Int J Cardiol 85: 33–49.
20. Okada K, Minamino T, Tsukamoto Y, Liao Y, Tsukamoto O, et al. (2004) Prolonged endoplasmic reticulum stress in hypertrophic and failing heart after aortic constriction: possible contribution of endoplasmic reticulum stress to cardiac myocyte apoptosis. Circulation 110: 705–712.
21. Thuerauf DJ, Marcinko M, Gude N, Rubio M, Sussman MA, et al. (2006) Activation of the unfolded protein response in infarcted mouse heart and hypoxic cultured cardiac myocytes. Circ Res 99: 275–282.
22. Qi X, Vallentin A, Churchill E, Mochly-Rosen D (2007) δPKC participates in the endoplasmic reticulum stress-induced response in cultured cardiac myocytes and ischemic heart. J Mol Cell Cardiol 43: 420–428.
23. Terai K, Hiramoto Y, Masaki M, Sugiyama S, Kuroda T, et al. (2005) AMP-activated protein kinase protects cardiomyocytes against hypoxic injury through attenuation of endoplasmic reticulum stress. Mol Cell Biol 25: 9554–9575.
24. Azfer A, Niu J, Rogers LM, Adamski FM, Kolattukudy PE (2006) Activation of endoplasmic reticulum stress response during the development of ischemic heart disease. Am J Physiol Heart Circ Physiol 291: H1411–1420.
25. Szegezdi E, Duffy A, O'Mahoney ME, Logue SE, Mylotte LA, et al. (2006) ER stress contributes to ischemia-induced cardiomyocyte apoptosis. Biochem Biophys Res Commun 349: 1406–1411.
26. Vitadello M, Penzo D, Petronilli V, Michieli G, Gomirato S, et al. (2003) Overexpression of the stress protein Grp94 reduces cardiomyocyte necrosis due to calcium overload and simulated ischemia. FASEB J 17: 923–925.
27. Martindale JJ, Fernandez R, Thuerauf D, Whittaker R, Gude N, et al. (2006) Endoplasmic reticulum stress gene induction and protection from ischemia/reperfusion injury in the hearts of transgenic mice with a tamoxifen-regulated form of ATF6. Circ Res 98: 1186–1193.
28. Ron D, Walter P (2007) Signal integration in the endoplasmic reticulum unfolded protein response. Nat Rev Mol Cell Biol 8: 519–529.
29. Fu HY, Minamino T, Tsukamoto O, Sawada T, Asai M, et al. (2008) Overexpression of endoplasmic reticulum-resident chaperone attenuates cardiomyocyte death induced by proteasome inhibition. Cardiovasc Res 79: 600–610.
30. Yoshida H, Okada T, Haze K, Yanagi H, Yura T, et al. (2000) ATF6 activated by proteolysis binds in the presence of NF-Y (CBF) directly to the cis-acting element responsible for the mammalian unfolded protein response. Mol Cell Biol 20: 6755–6767.
31. Raggo C, Rapin N, Stirling J, Gobeil P, Smith-Windsor E, et al. (2002) Luman, the cellular counterpart of herpes simplex virus VP16, is processed by regulated intramembrane proteolysis. Mol Cell Biol 22: 5639–5649.
32. Kondo S, Murakami T, Tatsumi K, Ogata M, Kanemoto S, et al. (2005) OASIS, a CREB/ATF-family member, modulates UPR signalling in astrocytes. Nat Cell Biol 7: 186–194.
33. Stirling J, O'Hare P (2006) CREB4, a transmembrane bZip transcription factor and potential new substrate for regulation and cleavage by S1P. Mol Biol Cell 17: 413–426.
34. Zhang K, Shen X, Wu J, Sakaki K, Saunders T, et al. (2006) Endoplasmic reticulum stress activates cleavage of CREBH to induce a systemic inflammatory response. Cell 124: 587–599.
35. Omori Y, Imai J, Watanabe M, Komatsu T, Suzuki Y, et al. (2001) CREB-H: a novel mammalian transcription factor belonging to the CREB/ATF family and functioning via the box-B element with a liver-specific expression. Nucleic Acids Res 29: 2154–2162.
36. Horio T, Nishikimi T, Yoshihara F, Nagaya N, Matsuo H, et al. (1998) Production and secretion of adrenomedullin in cultured rat cardiac myocytes and nonmyocytes: stimulation by interleukin-1β and tumor necrosis factor-α. Endocrinology 139: 4576–4580.
37. Ogata T, Ueyama T, Isodono K, Tagawa M, Takehara N, et al. (2008) MURC, a muscle-restricted coiled-coil protein that modulates the Rho/ROCK pathway, induces cardiac dysfunction and conduction disturbance. Mol Cell Biol 28: 3424–3436.
38. Kitamura R, Takahashi T, Nakajima N, Isodono K, Asada S, et al. (2007) Stage-specific role of endogenous Smad2 activation in cardiomyogenesis of embryonic stem cells. Circ Res 101: 78–87.
39. Asada S, Takahashi T, Isodono K, Adachi A, Imoto H, et al. (2008) Downregulation of Dicer expression by serum withdrawal sensitizes human endothelial cells to apoptosis. Am J Physiol Heart Circ Physiol 295: H2512–2521.
40. Guo W, Wong S, Xie W, Lei T, Luo Z (2007) Palmitate modulates intracellular signaling, induces endoplasmic reticulum stress, and causes apoptosis in mouse 3T3-L1 and rat primary preadipocytes. Am J Physiol Endocrinol Metab 293: E576–586.
41. Harada K, Ogai A, Takahashi T, Kitakaze M, Matsubara H, et al. (2008) Crossveinless-2 controls bone morphogenetic protein signaling during early cardiomyocyte differentiation in P19 cells. J Biol Chem 283: 26705–26713.

Pressure-Mediated Hypertrophy and Mechanical Stretch Induces IL-1 Release and Subsequent IGF-1 Generation to Maintain Compensative Hypertrophy by Affecting Akt and JNK Pathways

Shoken Honsho,* Susumu Nishikawa,* Katsuya Amano, Kan Zen, Yasushi Adachi, Eigo Kishita, Akihiro Matsui, Asako Katsume, Shinichiro Yamaguchi, Kenichiro Nishikawa, Kikuo Isoda, David W.H. Riches, Satoaki Matoba, Mitsuhiko Okigaki, Hiroaki Matsubara

Rationale: It has been reported that interleukin (IL)-1 is associated with pathological cardiac remodeling and LV dilatation, whereas IL-1β has also been shown to induce cardiomyocyte hypertrophy. Thus, the role of IL-1 in the heart remains to be determined.

Objective: We studied the role of hypertrophy signal-mediated IL-1β/insulin-like growth factor (IGF)-1 production in regulating the progression from compensative pressure-mediated hypertrophy to heart failure.

Methods and Results: Pressure overload was performed by aortic banding in IL-1β–deficient mice. Primarily cultured cardiac fibroblasts (CFs) and cardiac myocytes (CMs) were exposed to cyclic stretch. Heart weight, myocyte size, and left ventricular ejection fraction were significantly lower in IL-1β–deficient mice (20%, 23% and 27%, respectively) than in the wild type 30 days after aortic banding, whereas interstitial fibrosis was markedly augmented. DNA microarray analysis revealed that IGF-1 mRNA level was markedly (≈50%) decreased in the IL-1β–deficient hypertrophied heart. Stretch of CFs, rather than CMs, abundantly induced the generation of IL-1β and IGF-1, whereas such IGF-1 induction was markedly decreased in IL-1β–deficient CFs. IL-1β released by stretch is at a low level unable to induce IL-6 but sufficient to stimulate IGF-1 production. Promoter analysis showed that stretch-mediated IL-1β activates JAK/STAT to transcriptionally regulate the IGF-1 gene. IL-1β deficiency markedly increased c-Jun N-terminal kinase (JNK) and caspase-3 activities and enhanced myocyte apoptosis and fibrosis, whereas replacement of IGF-1 or JNK inhibitor restored them.

Conclusions: We demonstrate for the first time that pressure-mediated hypertrophy and mechanical stretch generates a subinflammatory low level of IL-1β, which constitutively causes IGF-1 production to maintain adaptable compensation hypertrophy and inhibit interstitial fibrosis. (*Circ Res.* 2009;105:1149-1158.)

Key Words: interleukin-1 ■ insulin-like growth factor-1 ■ Akt ■ JNK ■ hypertrophy

Cardiac hypertrophy is defined by augmentation of the ventricular mass against hemodynamic loads and up-regulates contractile capacity and reduces ventricular wall stress,[1] whereas the capacity of this compensation is limited, and stronger and longer pressure overload induces pathological cardiac remodeling with left ventricular (LV) dilatation.[1] Pathological cardiac remodeling is associated with production of the extracellular matrix and causes increased signals of myocyte apoptosis.[2]

Receptor tyrosine kinase, such as insulin-like growth factor (IGF)-1 receptor is involved in not only physiological hypertrophy[3] but also compensated hypertrophy after pressure overload.[4] IGF-1 promotes myocardial hypertrophy by activating phosphatidylinositol 3-kinase (PI3K) and its downstream effector Akt.[5,6] In addition, mitogen-activated protein kinase[7] acts as downstream molecules to promote hypertrophy.

Overexpression of G protein–coupled 7-transmembrane receptors in the heart induced cardiac remodeling, resulting in heart failure with increased propensity toward apoptosis and fibrosis.[8] Stress-activated mitogen-activated protein kinase, JNK (c-Jun N-terminal kinase), was reported to transmit this

Original received November 7, 2008; resubmission received August 30, 2009; revised resubmission received September 28, 2009; accepted October 6, 2009.

From the Department of Cardiovascular Medicine (S.H., S.N., K.A., K.Z., E.K., A.M., A.K., S.Y., S.M., M.O., H.M.), Kyoto Prefectural University of Medicine, Japan; Department of Pathology I (Y.A.), Kansai Medical University, Osaka, Japan; Internal Medicine-1 (K.N., K.I.), National Defense Medical College, Saitama, Japan; and Department of Pediatrics (D.W.H.R.), National Jewish Medical and Research Center, Denver, Colo.

*Both authors contributed equally to this work.

Correspondence to Mitsuhiko Okigaki, MD, Department of Cardiovascular Medicine, Kyoto Prefectural University of Medicine, Kamigyo-ku, Kyoto, 602-8566, Japan. E-mail okigakim@koto.kpu-m.ac.jp

Circulation Research is available at http://circres.ahajournals.org

DOI: 10.1161/CIRCRESAHA.109.208199

Non-standard Abbreviations and Acronyms	
CF	cardiac fibroblast
CM	cardiomyocyte
ERK	extracellular signal-regulated kinase
FS	fractional shortening
IGF	insulin-like growth factor
IL	interleukin
JAK	Janus kinase
JNK	c-Jun N-terminal kinase
LV	left ventricular
PCR	polymerase chain reaction
PI3K	phosphatidylinositol 3-kinase
ROS	reactive oxygen species
STAT5	signal transducer and activator of transcription 5
TNF	tumor necrosis factor
WT	wild type

action and transgenic mice of JNK induced cardiac fibrosis and apoptosis.[9] JNK inhibited NFATc3 (nuclear translocation of the transcription factor), which is involved in myocardial hypertrophy, leading to impaired LV hypertrophy.[10] Thus, the balance between the IGF-1/Akt system and JNK activation seems to be important to determine the fate of pressure-overloaded heart, ie, compensated hypertrophy or pathological cardiac remodeling; however, the interaction between these pathways has not been fully clarified.

Numerous data demonstrated that a proinflammatory cytokine, interleukin (IL)-1, is associated with inhibition of IGF-1 production and IGF-1-mdiated protein synthesis.[11,12] IL-1β has a negative inotropic effect on the heart[13] and produces extracellular matrix to promote pathological cardiac remodeling and LV dilatation.[14,15] There are reports showing that IL-1β promotes myocyte hypertrophy[16,17] and that cardiac-targeted IL-1α overexpression mice exhibit concentric LV hypertrophy with preserved LV systolic function.[18] Thus, the role of IL-1β in the heart remains to be determined.

In this study, we found that compensated LV hypertrophy during pressure overload was attenuated in IL-1β–deficient mice. Further analysis revealed that a low level of IL-1β is constitutively produced by mechanical stretch of cardiac fibroblasts (CFs), as well as cardiac myocytes (CMs). Unexpectedly, DNA microarray and gene promoter analysis showed that the stretch-mediated IL-1β release promotes IGF synthesis transcriptionally through the JAK2/STAT5 (Janus kinase 2/signal transducer and activator of transcription 5) pathway. IGF-1 inhibited stretch-induced JNK activation, myocyte apoptosis, or interstitial fibrosis and stimulated Akt-mediated signals, contributing to compensated LV hypertrophy in the initial phase after pressure overload.

Methods

Materials and Methods for animal models, transthoracic echocardiography, pathology, Western Blotting, cell culture, mechanical stretch, microarray analysis, RNA isolation and real-time polymerase chain reaction (PCR), Luciferase assay, small interfering RNA knockdown of IL-1α, immunostaining, quantifications for IL-1β and IGF-1 protein, oxidative stress, apoptosis, and data analysis are described in the Online Data Supplement.

Results

IL-1β Maintains Pressure-Mediated LV Hypertrophy

LV hypertrophy was induced by aortic banding. The ratio of heart weight/body weight ratio (mg/g) and the myocyte size in a cross-sectional area were significantly smaller (20.2% and 23.3%, respectively, at day 30) in IL-1β–deficient mice compared with the wild type (WT) (Figure 1A), whereas the ratio of lung weight/body weight was similar between WT and IL-1β–deficient mice (6.8±0.3 versus 6.1±0.1 mg/g). Echocardiographic evaluation showed that the LV diastolic diameters in IL-1β–deficient mice at day 30 and day 60 were significantly larger (19.5% and 25.1% versus WT, respectively) and percentage fractional shortening (%FS) was lower (17.4% and 26.5%) (Figure 1B), although these baseline parameters were similar between groups.

Posterior and anterior wall diameters at day 60 were ≈38% smaller in IL-1β–deficient LV than the WT (posterior wall diameter: 0.8±0.04 versus 1.1±0.08 mm; anterior wall diameter: 0.8±0.06 versus 1.1±0.07 mm; each $P<0.05$), although there was no significant difference in the baseline (0.7±0.04 mm in both groups). The interstitial fibrosis in IL-1β–deficient LV was markedly increased (3.1-fold at day 60) compared with the WT (Figure 1C). Atrial natriuretic peptide and β-myosin heavy chain mRNA levels were increased in hypertrophied hearts of WT (3.7- and 3.5-fold, respectively), whereas, in IL-1β–deficient mice, mRNA levels were increased to a significantly less extent (38.2% and 32.2% versus WT) (Figure 1D).

Hypertrophy Stimulus Causes IGF-1 Production via IL-1β Release

To identify the molecules involved in IL-1β–mediated cardiac hypertrophy, we analyzed the transcripts from LV samples 3 days after aortic banding using a DNA oligonucleotide microarray approach. Interestingly, we found that IGF-1 was one of the molecules in which the mRNA level was markedly (≈38%) reduced in IL-1β–deficient mice. Indeed, the baseline mRNA level of IGF-1 was 51% lower in IL-1β–deficient LV. Pressure overload induced a 1.9-fold increase in IGF-1 mRNA in WT left ventricles (day 14 versus baseline), whereas, in IL-1β–deficient mice, the increase was markedly attenuated (Figure 2A, left). Cardiac IGF-1 protein levels at day 0 (baseline), day 14 and day 60 after aortic banding were ≈60% lower in IL-1β–deficient mice compared with the WT. When Histidine (His)-tagged IGF-1 (50 μg/kg per day, once per day) was subcutaneously injected into IL-1β–deficient mice after aortic banding, we found that His-IGF-1 levels increased to the plateau at day 14 and total (exogenous His-IGF-1 plus endogenous) IGF-1 amounts were elevated to the levels similar to the WT (Figure 2A, middle). Immunostaining revealed that IGF-1 protein is expressed in both myocytes and interstitial cells, the level of which appeared to be lower in IL-1β–deficient mice (Figure 2A, right). Phosphorylation levels of cardiac IGF-1 receptor were significantly lower (55% to 50% versus WT) in IL-1β–

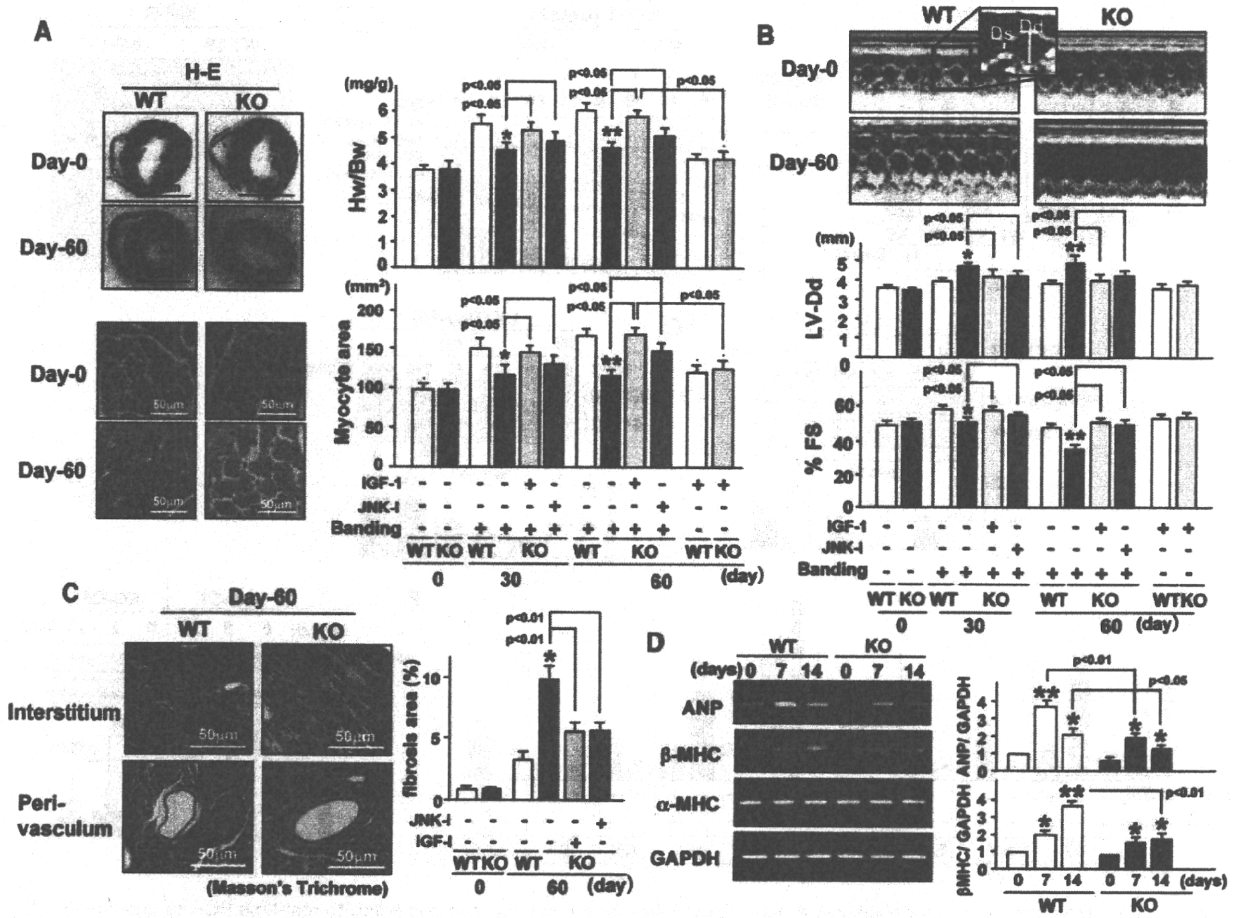

Figure 1. Impaired compensative LV hypertrophy in IL-1β–deficient mice. Abdominal aorta of WT or IL-1β–deficient mice (KO) was banded (day 0), and thereafter mice were subcutaneously injected with or without IGF-1 (50 μg/kg per day, once per day for 14 days). A, Hearts were removed and the ratio of heart weight/body weight ratio (Hw/Bw) (mg/g) was evaluated. Paraffin-sectioned left ventricles were stained with hematoxylin/eosin (H-E), and cross-sectional areas of cardiomyocytes were evaluated. *P<0.05, **P<0.01 vs WT (n=15). B, Echocardiography. Dd indicates end-diastolic diameter; Ds, end-systolic diameter. %FS was calculated as described in the Online Data Supplement. *P<0.05, **P<0.01 vs WT (n=10). C, Paraffin-sectioned left ventricles were stained with Masson's trichrome to evaluate the fibrotic area (arrows). *P<0.01 vs WT (n=7). D, Total RNAs were extracted from left ventricles. Atrial natriuretic peptide (ANP), α-myosin heavy chain (αMHC), α-myosin heavy chain (βMHC), and GAPDH mRNA levels were evaluated by quantitative RT-PCR. *P<0.05, **P<0.01 vs baseline (day 0) (n=5).

deficient mice after aortic banding, and treatment with 50 μg/kg per day of IGF-1 for 14 days normalized the decreased phosphorylation, whereas more than 250 μg/kg per day of IGF-1 caused the superphosphorylation over the normal level (Figure 2C).

We further studied whether exogenous IGF-1 reverses cardiac phenotype in IL-1β–deficient mice. Subcutaneous injection of IGF-1 (50 μg/kg per day, once per day) for 14 days restored the phosphorylation level of cardiac IGF-1 receptor to the WT level, whereas more than 250 μg/kg per day of IGF-1 caused the phosphorylation over the normal level, suggesting that 50 μg/kg per day of IGF-1 is not an excess amount, and this infused amount likely induces a physiological response of IGF-1 receptor (Figure 2C). Daily injection of IGF-1 (50 μg/kg per day) to IL-1β deficient mice without aortic banding for 60 days increased the heart/body weight ratio by 10% and myocyte area by 22% greater than the baseline (each P<0.05) (Figure 1A), whereas cardiac parameters did not significantly change (Figure 1B). In contrast, banding+IGF-1 treatment induced an even more effect at day 60 (20% increase in the heart/body weight ratio and 41% in myocyte area versus banding without IGF-1) (Figure 1A). Cardiac function in IL-1β–deficient mice with aortic banding was depressed at day 60 (18% decrease in %FS and 36% enlargement of LV dimension versus baseline) and IGF-1 treatment significantly improved the LV dysfunction (35% increase in %FS and 19% inhibition of LV dilatation) (Figure 1B).

To study the involvement of IGF-1 in the hypertrophy process, we examined whether cyclic stretch (60 cycle/min at 12% extension)[19] can affect IGF-1 expression. As we found that stretch-mediated IGF-1 generation is much greater in CFs than CMs (Figure 2D), the primarily cultured CFs was used in the following stretch experiment. Stretch induced IGF-1 mRNA accumulation (4.1-fold versus baseline) and IGF-1 protein synthesis (3.6-fold) in WT CFs, and this increase in IGF-1 protein level was abolished by anti–IL-1β neutralization antibody, whereas in IL-1β–deficient CFs, the stretch-mediated increase was markedly lower (49% versus WT CFs) (Figure 2D). Stretch caused a phosphorylation of

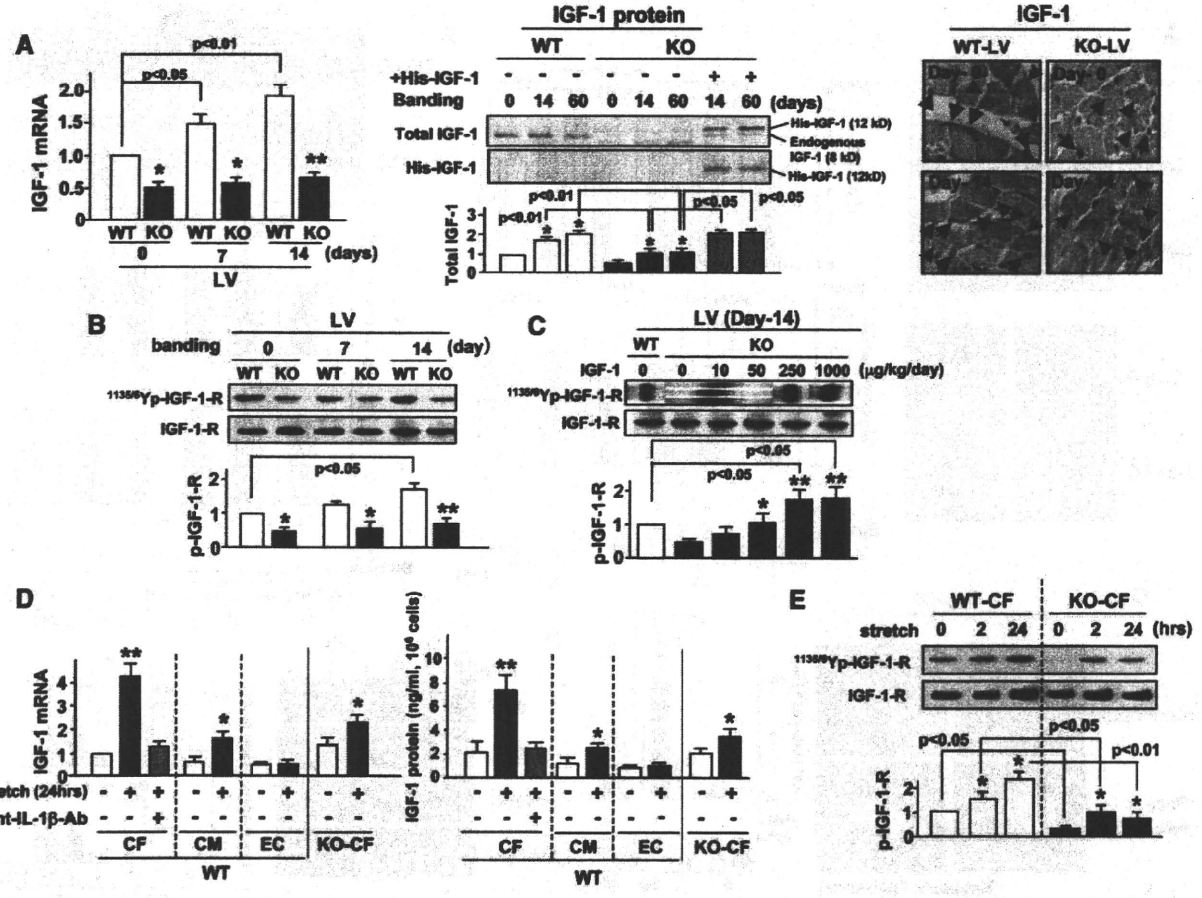

Figure 2. IGF-1 expression in IL-1β deficiency. A (left), Total RNAs were extracted and subjected to real-time PCR to quantify IGF-1 mRNA levels. *$P<0.01$, **$P<0.005$ vs WT (n=6, each). A (middle), LV lysates from mice treated with or without histidine-tagged (His-tag) IGF-1 (50 μg/kg per day, once a day) were analyzed by Western blotting using anti–IGF-1 and anti–His tag antibodies. *$P<0.05$ vs baseline (n=4). A (right), Frozen sections were immunostained with anti–IGF-1 antibody and counterstained with hematoxylin/eosin. IGF-1–positive interstitial cells (arrows) or cardiomyocytes (arrowheads) are indicated. B and C, LV lysates from mice treated with or without daily injection of IGF-1 were immunoblotted with antibodies for IGF-1 receptor (IGF-1-R) and Tyr1135/1136-phoshorylated IGF-1 receptor. *$P<0.05$, **$P<0.01$ vs WT left ventricles (n=5, each) (B); *$P<0.05$, **$P<0.01$ vs baseline (n=5, each) (C). D, CFs, CMs, or endothelial cells (EC) were exposed to cyclic stretch (60 cycle/min) for 24 hours by 12% extension with or without neutralizing anti–IL-1β antibody (1 μg/mL). Total RNAs were subjected to real-time PCR to quantify IL-1β mRNA. Also, IGF-1 protein in incubation medium was analyzed by ELISA. *$P<0.05$, **$P<0.01$ vs baseline in each genotype (n=5, each). E, Cell lysates were analyzed by Western blotting with antibodies against IGF-1 receptor or Tyr1135/1136-phoshorylated IGF-1 receptor. *$P<0.05$ vs baseline in each genotype.

IGF-1 receptor, the extent of which was significantly greater in WT CFs than IL-1β–deficient CFs (Figure 2E).

IL-1β Is Produced by Stretch to Stimulate IGF-1 Generation

We next studied whether IL-1β expression is actually induced by aortic banding or cyclic stretch. IL-1β mRNA was expressed in LV and the level was increased ≈2.0-fold after aortic banding, and immunohistochemistry revealed that IL-1β protein is detectable in both myocytes and interstitial cells (Figure 3A). Stretch also induced IL-1β mRNA accumulation in both CFs and CMs in parallel with percentage extension and duration of stretch, whereas the amount of IL-1β mRNA produced by CFs was 2.2-fold higher than CMs (Figure 3B). The significant induction of IL-1β mRNA was observed 3 hours after stretch and the level reached to a peak around 6 hours (Figure 3B, right).

We also measured the concentration of IL-1β released by stretch and found that a substantial amount of IL-1β (≈1.2 ng/mL) was detected in the condition medium derived from 24-hour stretched CFs, the level of which was much lower than that in the condition medium (≈5.1 ng/mL) from a sepsis-associated inflammatory cytokine tumor necrosis factor (TNF)α-treated (1 ng/mL, 24-hour exposure) CFs (Figure 3C). Because plasma TNFα was shown to increase to ≈1 ng/mL in patients with sepsis,[20] we examined the effects of 1 and 10 ng/mL TNFα in this experiment (Figure 3C). We found that incubation medium containing IL-1β released by stretch barely induced an inflammatory cytokine IL-6 expression from CFs, whereas the condition medium from TNFα-treated (1 ng/mL) CFs abundantly stimulated IL-6 synthesis and this action was abolished by neutralization with anti–IL-1β antibody (Figure 3D).

We further studied whether IL-1β actually stimulates IGF-1. IGF-1 synthesis in WT CFs and WT CMs was maximally induced by 10 ng/mL IL-1β, but downregulated with 20 ng/mL IL-1β, suggesting that CFs and CMs were

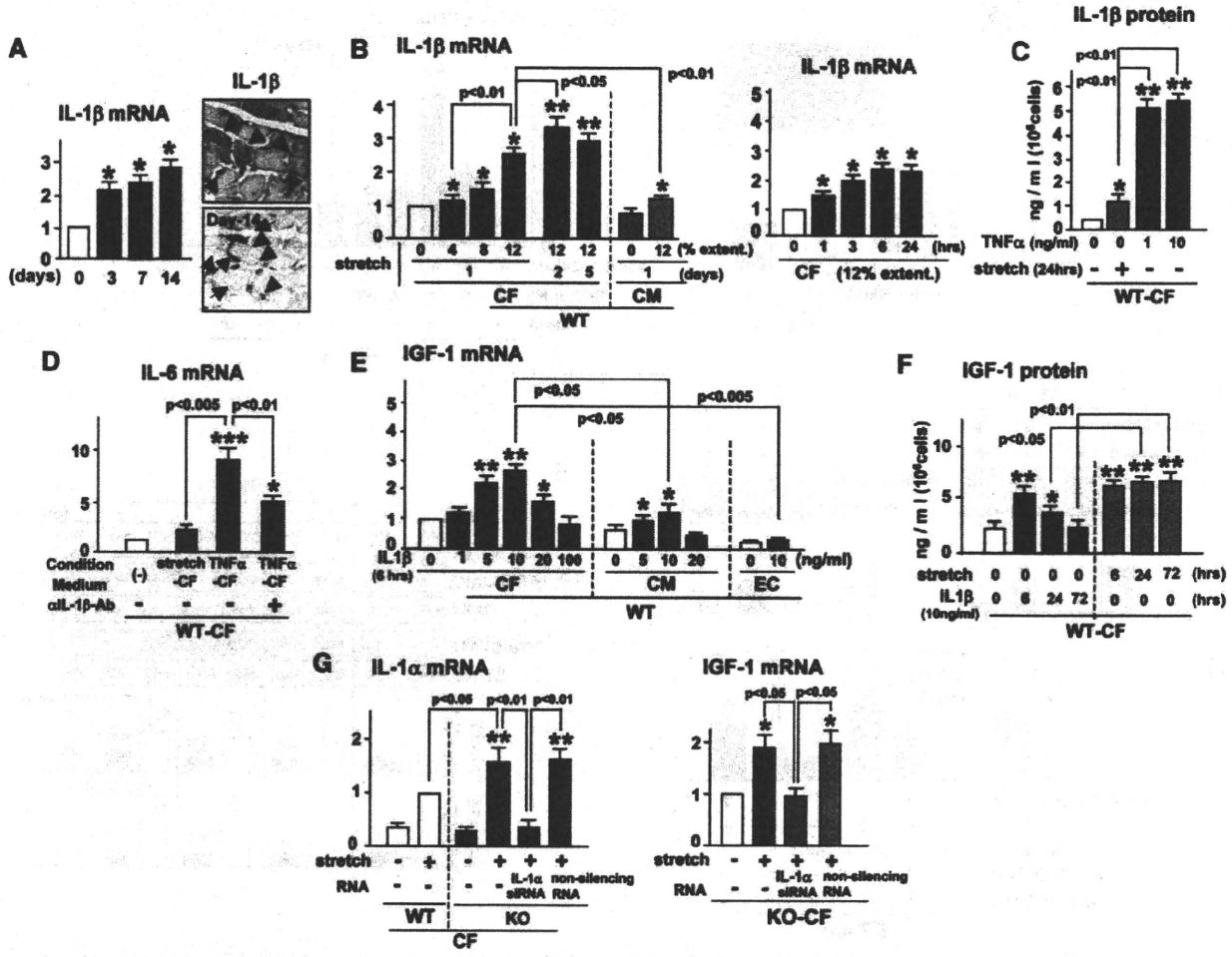

Figure 3. Low level of IL-1β constitutively produced by mechanical stretch induces IGF-1 generation. A, IL-1β mRNA was quantified by real-time PCR analysis. Frozen-sectioned samples were immunostained by anti–IL-1β antibody. B, CFs and CMs were exposed to cyclic stretch (0% to 12% extension, 60 cycles/min) for indicated time. Total RNA was subjected to real-time PCR to quantify IL-1β mRNA. C, CFs were cyclically stretched (60 cycles/min, 12% extension) or stimulated with TNFα (1 ng/mL or 10 ng/mL) for 24 hours. IL-1β protein in incubation medium was analyzed by ELISA. D, CFs were incubated for 24 hours with condition medium derived from the CFs pretreated with cyclic stretch for 24 hours or with TNFα (1 ng/mL) for 24 hours. Total RNA was extracted and subjected to real-time PCR to quantify IL-6 mRNA. E, CFs, CMs, or endothelial cells (EC) were stimulated with IL-1β (0 to 100 ng/mL) or cyclic stretch for 6 hours. Total RNAs or supernatants were analyzed by real-time PCR or ELISA to quantify IGF-1 mRNA or IGF-1 protein levels. F, CFs were stimulated with IL-1β (10 ng/mL) or cyclic stretch for the indicated time. IGF-1 protein in incubation medium was analyzed by ELISA. $^*P<0.05$, $^{**}P<0.01$, $^{***}P<0.005$ (vs baseline, n=4 each) (A through F). G, CFs were exposed to cyclic stretch for 24 hours with or without small interfering RNA (siRNA) for IL-1α or nonsilencing RNA (50 nmol/L in final concentration). Total RNA were analyzed by real-time PCR for quantification of IL-1α or IGF-1 mRNA. $^*P<0.05$, $^{**}P<0.01$ vs baseline.

responsive to IL-1β in a similar dose-responsive manner (Figure 3E). IL-1β–mediated (10 ng/mL) induction of IGF-1 mRNA was much greater (>2-fold) in WT CFs compared with WT CMs and no induction was observed in endothelial cells (Figure 3E). IL-1β (10 ng/mL) stimulated the release of IGF-1 protein with a peak at 6-hour exposure and thereafter decreased, whereas stretch-mediated IGF-1 protein release was sustained over 72 hours (Figure 3F). CFs produced ≈1.2 ng/mL IL-1β under stretch (Figure 3C), whereas nonstretched CFs did not respond to 1 ng/mL IL-1β and required >5 ng/mL IL-1β to induce a significant increase in IGF-1 mRNA (Figure 3E), suggesting that there is a differential sensitivity to IL-1β between stretched and nonstretched CFs and mechanical stretch elevates the sensitivity to IL-1β. We therefore stimulated the nonstretched CFs with 10 ng/mL IL-1β in the following experiments.

We also examined an involvement of IL-1α in IL-1β deficiency. After 24-hour stretch of IL-1β–deficient CFs, IL-1α mRNA levels were increased 1.8-fold compared with WT CFs (Figure 3G). Knockdown of IL-1α by small interfering RNA in IL-1β–deficient CFs completely abolished the stretch-induced increase in IGF-1 mRNA (Figure 3G), indicating that IL-1α partially compensates for IGF-1 induction in IL-1β deficiency.

Reactive Oxygen Species Is Needed for Stretch-Mediated IL-1β Induction

Reactive oxygen species (ROS) has been shown to be involved in stretch-mediated cytokine induction in the heart.[21] Intracellular ROS levels evaluated by the production of 2′,7′-dichlorofluorescein (DCF) were markedly increased (4.2-fold versus nonstretched baseline) after 24-hour stretch

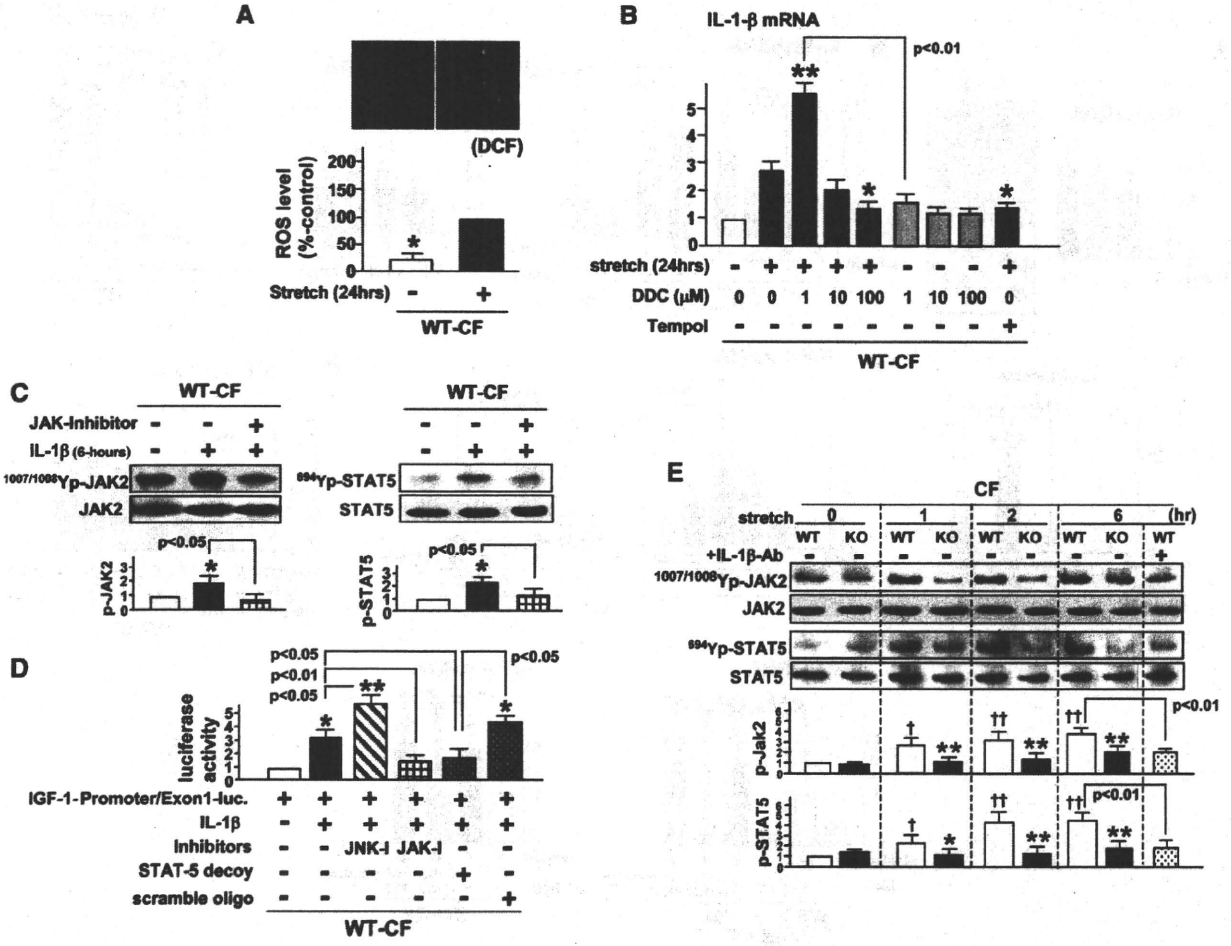

Figure 4. Role of ROS in stretch-induced IL-1β generation and JAK2/STAT5 in IL-1β-induced IGF-1. A, WT CFs were cyclically stretched for 24 hours, and intracellular ROS level was evaluated as the production of 2′,7′-dichlorofluorescein (DCF). *P<0.01 vs 24-hour stretched WT (set as 100%) (n=4, each). B, WT CFs were exposed to cyclic stretch for 24 hours with or without diethyldithiocarbamate (DDC) or Tempol (1 mmol/L). *P<0.05, **P<0.01 vs baseline (n=4 each). C, WT CFs were stimulated with IL-1β (10 ng/mL) for 30 minutes with or without JAK inhibitor (AG490, 10 μmol/L). Cell lysates were subjected to Western blotting. *P<0.05, **P<0.01 vs baseline (n=4 each). D, Luciferase reporter gene construct containing mouse IGF-1 gene promoter and exon 1 (−1711 to +329) was transfected into WT CFs with or without STAT5 decoy or scramble oligonucleotide (1 μg/mL final concentration) or inhibitors of JAK or JNK. At 24 hours after transfection, cells were stimulated with IL-1β (10 ng/mL) for 6 hours and luciferase activity was measured. *P<0.01, **P<0.005 vs baseline (n=4 each). E, CFs were exposed to cyclic stretch (60 cycles/min, 12%) with or without anti–IL-1β neutralizing antibody (1 μg/mL). Cell lysates were subjected to Western blotting using antibodies against Tyr1007/1008-phosphorylated JAK2, JAK2, Tyr694-phosphorylated STAT5, or STAT5. *P<0.05, **P<0.01 vs WT CFs (n=4 each). †P<0.05, ††P<0.01 vs WT CFs at baseline (n=4 each).

of WT CFs (Figure 4A, left). A low dose of diethyldithiocarbamate (1 μmol/L), which increases the intracellular ROS level by inhibiting Cu/Zn-superoxide dismutase,[22] augmented stretch-mediated IL-1β mRNA levels (2.0-fold versus control), whereas 1 to ≈100 μmol/L diethyldithiocarbamate without stretch did not affect these levels and scavenging ROS by Tempol (1 mmol/L) markedly reduced stretch-mediated IL-1β mRNA accumulation (58% versus control) (Figure 4B, right). These findings indicate that intracellular ROS is closely involved in stretch-mediated IL-1β production.

IL-1β Induces IGF-1 Through JAK2/STAT5 Pathway

IGF-1 release by growth hormone is reportedly activated by the JAK2/STAT5 pathway.[23] Stimulation of WT CFs with IL-1β significantly induced the phosphorylation of JAK2 and STAT5 by 2.1- and 2.3-fold, respectively, and JAK inhibitor (AG490, 100 μmol/L) abolished the phosphorylation of STAT5 (Figure 4C). We also found that the stretch-mediated induction of IL-1β and IGF-1 was abolished by pretreatment of Tempol and AG490 (data not shown), suggesting that the induction of IL-1β/IGF-1 by mechanical stretch is regulated with the same signaling between CFs and CMs.

Transcription of IGF-I is positively regulated by the 5′ noncoding region flanking IGF-1 exon 1,[24] and STAT5-binding sites are identified in this region.[25] To study the role of STAT5 in IL-1-mediated IGF-1 transcription, a luciferase reporter gene construct containing mouse IGF-1-gene promoter and exon-1 (−1711 to +329) was introduced to WT CFs with or without STAT5 decoy or scramble oligonucleotides. Stimulation of WT CFs with IL-1β for 6 hours induced

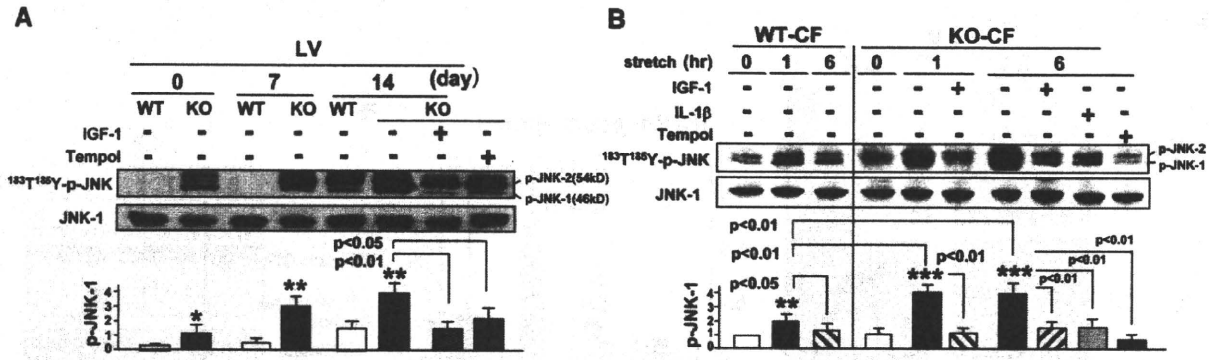

Figure 5. IL-1β/IGF-1 deficiency induces JNK activation. A, Left ventricles were removed 7 or 14 days after banding aorta with or without administration of IGF-1 (50 μg/kg per day for 14 days) or ROS scavenger, Tempol (300 μmol/kg per day), and cell lysates were subjected to Western blotting. *$P<0.01$, **$P<0.005$ vs WT (n=5 each). B, CFs were stretched for the indicated time with or without IGF-1 (5 ng/mL) or IL-1β (1.5 ng/mL). Cell lysates were analyzed by Western blotting. *$P<0.05$, **$P<0.01$, ***$P<0.005$ vs baseline in each genotype (n=5 each).

transcriptional activity (3.2-fold versus baseline), whereas JAK inhibitor and STAT5 decoy abolished this IL-1β-mediated action (Figure 4D).

Furthermore, stretch-induced phosphorylations of JAK2 and STAT5 was severely inhibited in IL-1β–deficient CFs (JAK2, 51.2%; STAT5, 59.3% reduction versus WT CFs at 6-hour stretch) or the addition of neutralizing anti–IL-1β antibody (JAK2, 49.7%; STAT5, 52.4% reduction) (Figure 4E).

IL-1α Receptor Signaling Augments IGF-1 Synthesis and LV Hypertrophy

We further studied the hypertrophy-mediated IGF-1 expression using CM-specific IL-1α overexpression transgenic mice). Although cardiac size and function in IL-1α transgenic mice at baseline did not differ from the WT, the heart/body weight ratio and myocyte area were more increased ($P<0.05$ versus WT) 60 days after aortic banding. %FS was 18% better ($P<0.05$ versus WT), and LV dilatation was reduced 14% (Online Figure I, A and B). IGF-1 mRNA levels in LV were significantly increased at the baseline and after aortic banding (2.2-fold at day 7) (Online Figure I, C), and Tyr1135/1136 phosphorylation levels of IGF-1 receptor were also elevated (2.3-fold) (Online Figure I, D). Considering that IL-1α binds to the receptor in common with IL-1β, these findings suggest that hypertrophy stimuli and IL-1 signals are sufficient to induce IGF-1 expression.

IL-1β Deficiency Activates JNK

JNK is closely involved in the development of myocyte apoptosis and cardiac fibrosis.[9] Basal JNK activities were markedly increased in IL-1β–deficient LV and further stimulated after aortic banding, which was markedly inhibited by addition of IGF-1 or Tempol (Figure 5A). JNK activities in CFs increased to the peak level 1 hour after stretch and, thereafter, decreased to the baseline, whereas the level was higher and sustained for 6 hours in IL-1β–deficient CFs, and this induction was abolished by addition of IGF-1 and IL-1β or Tempol (Figure 5B). Consistent with these findings, subcutaneous injection of JNK inhibitor (SP600125, 30 mg/kg per day) to IL-1β–deficient mice after aortic banding showed that JNK inhibitor restored cardiac dysfunction, such as LV dilatation and decreased %FS, to the WT levels at day 60 (Figure 1B), accompanied by normalization of heart/body weight ratio and myocyte area (Figure 1A).

IL-1β–Mediated IGF-1 Generation and Cardiac Akt and ERK Activities

IGF-1 is known to promote LV hypertrophy through the extracellular signal-regulated kinase (ERK) or PI3K/Akt-1 pathway.[7] CFs is a main source for IL-1β-mediated IGF-1 generation, which has an effect on CMs in a paracrine fashion. Therefore, we next examined the effect of IGF-1 on the Akt/Erk pathway using the CMs. Phosphorylation levels of Akt and ERK after aortic banding and stretch stimulus were markedly decreased in IL-1β–deficient LV (59% and 79% at day 14, respectively) and IL-1β–deficient CMs (62% and 65% at 6 hours of stretch, respectively), whereas addition of IGF-1 normalized the decrease (Online Figure II, A and B). Treatment of WT CMs with anti–IL-1β antibody significantly diminished the phosphorylation levels of ERK and Akt-1 (48% and 53%, respectively) (Online Figure II, B). Thus, cardiac Akt and ERK activities in response to hypertrophy stimulus are attenuated in IL-1β–deficient mice, in which the lack of IGF-1 attributable to IL-1β deficiency is closely involved.

IL-1β Deficiency Causes JNK-Mediated Myocyte Apoptosis and Fibrosis

Inhibition of PI3K/Akt-1 and activation of JNK in the heart induces myocyte apoptosis[8] and fibrosis.[6] The number of TUNEL-positive cells in IL-1β–deficient LV was 3.1-fold greater (versus WT left ventricles) 14 days after aortic banding, and the subcutaneous administration of IGF-1 or JNK inhibitor (SP600125) normalized them (Figure 6A). JNK activates the mitochondrial apoptosis pathway through the caspase cascade.[7] Total and cleaved caspase-3 levels in IL-1β–deficient LV were markedly increased 7.2-fold and 2.7-fold 14 days after aortic banding, respectively, and the increase was abolished by administration of IGF-1 (Figure 6B).

Discussion

The present study demonstrates that pressure-mediated hypertrophy and mechanical stretch induce a low level of IL-1β

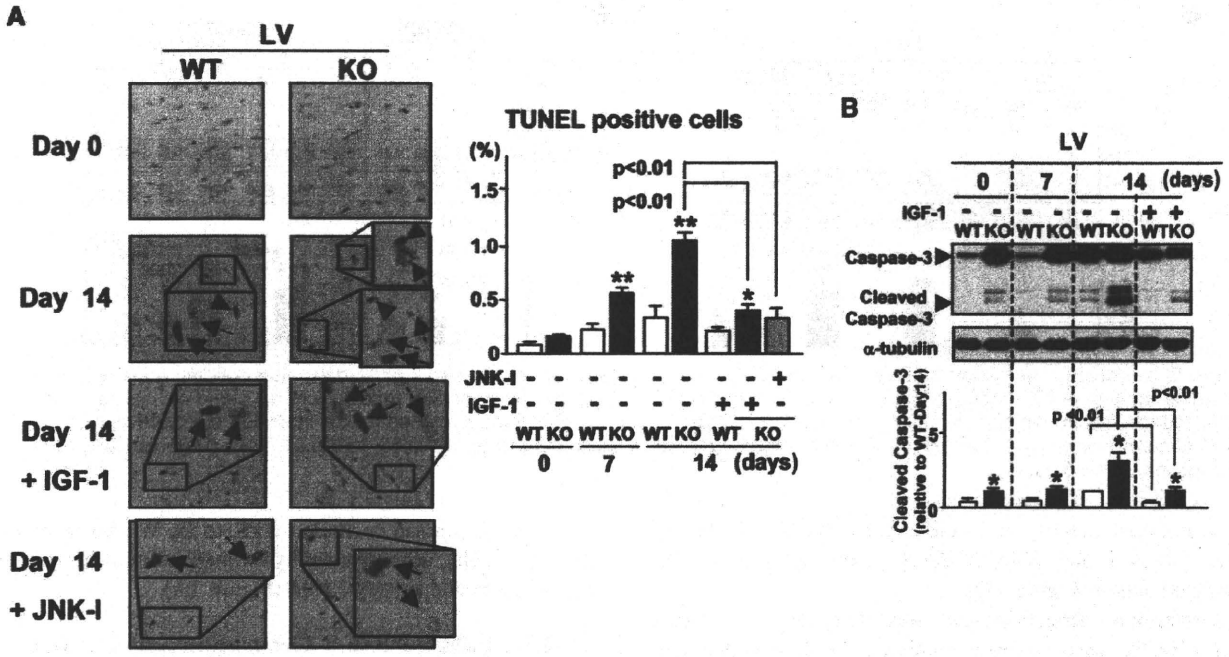

Figure 6. IL-1β/IGF-1 deficiency increases apoptosis. A, Left ventricles were removed 7 or 14 days after banding the aorta with or without administration of IGF-1 (50 μg/kg per day for 14 days) or JNK inhibitor (SP600125 [Calbiochem]; 10 μg/kg IP once per day for 14 days). Frozen-sectioned left ventricles were stained with TUNEL and counterstained with hematoxylin/eosin. Apoptotic cells were evaluated as TUNEL-positive cells. Arrows and broken arrows indicated apoptotic and nonapoptotic CMs, respectively, and arrowheads indicate apoptotic interstitial cells. *$P<0.05$, **$P<0.01$ vs WT (n=10 each). B, WT CMs were exposed to cyclic stretch with or without IGF-1 (50 ng/mL) for 24 hours. Total LV or cellular lysates were analyzed by Western blotting; relative values of cleaved caspase-3 to α-tubulin densities are shown (WT values at day 14 set as 1, n=5 each). *$P<0.05$ vs WT (n=5 each).

generation from both CFs and CMs to efficiently stimulate the synthesis and release of IGF-1 in an autocrine and/or paracrine fashion, leading to Akt-mediated compensative hypertrophic response of myocytes, as well as antiapoptotic and antifibrosis effects. Furthermore, we found that stretch-mediated ROS generation stimulated IL-1β generation and that IL-1β–mediated JAK/STAT activation transcriptionally induced IGF-I gene expression. Simultaneously, stretch stimulus markedly activated JNK, and IGF-1 generated by stretch negatively regulated JNK signals, resulting in the prevention of myocyte apoptosis and interstitial fibrosis, suggesting that the balance between hypertrophy stimulus-induced IL-1β/IGF-1 and subsequent JNK activation plays a key role to regulate the progression from adaptable compensation hypertrophy to heart failure (Figure 7).

IL-1β generated by sepsis or tissue inflammation has been reported to inhibit IGF-1 production.[11,12] What is the mechanism regulating the dual effect of IL-1β on IGF-1 generation? In this study, a physiological range of IL-1β generated by hypertrophic stimulus that caused IGF-1 synthesis was defined to be a low level of IL-1β (≈1 ng/mL), and a much higher level (over 10 fold) of IL-1β, such as generated by tissue inflammation,[26] that negatively regulated IGF-1 synthesis (Figure 3E) was defined to be a high level of IL-1. This low level of IL-1β was unable to induce proinflammatory cytokine IL-6 (Figure 3C and 3D), the amount of which can actively stimulate IGF-1 production sufficient to promote myocyte hypertrophy during pressure overload, as well as negatively regulate JNK activation. The study using STAT5 knockout mice indicated that STAT5 was required for both basal and growth hormone–induced expression of hepatic IGF-1.[27] We found that JAK2/STAT5 system is involved in IL-1β–mediated IGF-1 induction (Figure 4), whereas the higher level of IL-1β induced by endotoxin in sepsis was reported to rather inhibit STAT5-mediated IGF-1 production

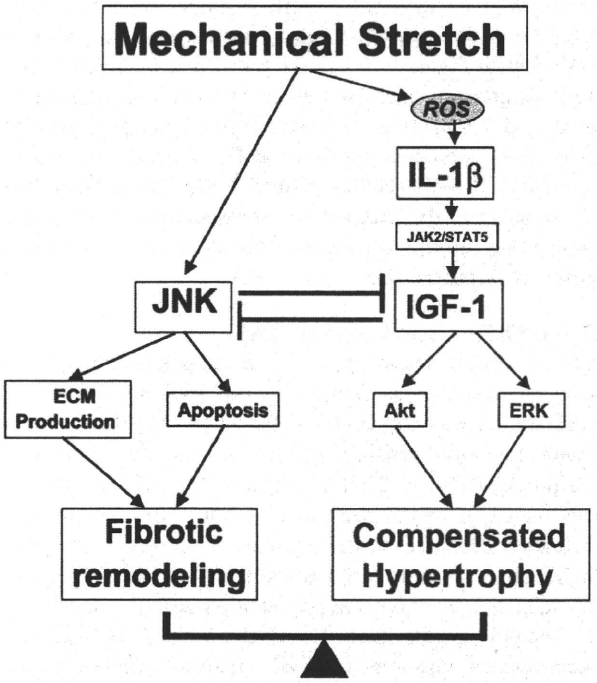

Figure 7. Role of stretch-mediated IL-1β/IGF-1 in pressure-overloaded heart.

through the activation of JNK.[28] The present study demonstrates that an appropriate level of ROS generation also plays an important role for stretch-mediated IL-1β production (Figure 4B).

IL-1β deficiency causes a decrease in IGF-1 synthesis, leading to reduction in pressure-induced LV hypertrophy associated with myocyte apoptosis and interstitial fibrosis (Figure 1) and JNK hyperactivity (Figure 5), whereas JNK inhibition restored cardiac function by decreasing cardiac apoptosis and fibrosis (Figure 6). Thus, JNK hyperactivity is closely involved in cardiac phenotype of IL-1β–deficient mice. The magnitude and duration of JNK activity are determined by the balance between activating kinases and inhibitory phosphatases for JNK. Catalytic cysteine of phosphatase is sensitive to oxidation. JNK phosphatase oxidation by ROS converts the catalytic cysteine to sulfenic acid and inhibits its activity, leading to sustained JNK activation.[29] We here showed that pulsating stretch induced ROS (Figure 4A), and ROS scavenger inhibits JNK activation (Figure 5), suggesting that ROS activates JNK in the heart. Considering that cardiac IGF-1 levels in IL-1β–deficient mice are >40% lower at baseline and after aortic banding than the WT (Figure 5), it is possible that IGF-1 prevents JNK hyperactivation under normal condition, as well as pressure-overload.

Which comes first to determine the cardiac phenotype in IL-1β–deficient mice, stimulation of JNK or downregulation of IL-1β ? We examined how JNK is affected after IGF-1 treatment. The result showed that exogenous IGF-1 normalized cardiac JNK hyperactivation in IL-1β–deficient mice (Figure 5). It was reported that IGF-1 receptor/Akt signaling inhibits JNK pathway.[30] Thus, it is considered that the downregulation of IL-1β/IGF-1 system is the upstream and subsequent hyperactivation of JNK is involved in the cardiac phenotype in IL-1β–deficient mice.

Calcineurin-dependent transcription factor, NFATc, promotes cardiac hypertrophy, and phosphorylation of NFATc by JNK inhibits its nuclear translocation and cardiac growth.[10] We found that stretch induced nuclear translocation of NFATc4, which was attenuated in IL-1β–deficient mice and JNK inhibition restored nuclear translocation of NFATc4 (Figure 6D), suggesting that JNK hyperactivation is closely involved in inhibition of pressure-overloaded hypertrophy in IL-1β–deficient mice.

The mechanism of striking increase of total caspase-3 has not been fully clarified in this study. Receptor tyrosine kinase, such as IGF-1 receptor, and its downstream Akt downregulates X-linked inhibitor of apoptosis protein (X-IAP), a ubiquitin–protein ligase, which promotes proteasomal degradation of caspase-3[31,32] Indeed, IGF-I attenuates caspase-3 activation and inhibits myocyte apoptosis,[33] suggesting that inhibition of IGF-1 receptor/Akt signaling in IL-1β–deficient mice leads to a decrease in degradation of caspase-3 followed by striking accumulation.

In conclusion, mechanical stretch constitutively induces a low level of IL-1β in the heart. This level of IL-1β is sufficient to induce IGF-1 production that negatively regulates JNK signals, affecting the progression of myocyte hypertrophy and subsequent transition from the compensated state to heart failure. The counterbalance of hypertrophy-induced IL-1/IGF-1 activation and the JNK pathway determines the fate of the pressure-overloaded heart: compensative hypertrophy or heart failure.

Acknowledgments

We thank Dr Sudo and Dr Iwakura for distribution of IL-1β knockout mice and Dr Ohsuzu for distribution of IL-1α transgenic mice.

Sources of Funding

This study was supported by grants-in-aid from the Ministry of Education, Science and Culture and from the Ministry of Health Labor and Welfare, Japan (grants 15590778, 18590822, and 20590884 to M.O.).

Disclosures

None.

References

1. Ruwhof C, van der Laarse A. Mechanical stress-induced cardiac hypertrophy: mechanisms and signal transduction pathways. *Cardiovasc Res.* 2000;47:23–37.
2. Heineke J, Molkentin JD. Regulation of cardiac hypertrophy by intracellular signalling pathways. *Nat Rev Mol Cell Biol.* 2006;7:589–600.
3. Welch S, Plank D, Witt S, Glascock B, Schaefer E, Chimenti S, Limana F, Leri A, Kajstura J, Anversa P, Sussman MA. Cardiac-specific IGF-1 expression attenuates dilated cardiomyopathy in tropomodulin-overexpressing transgenic mice. *Circ Res.* 2002;90:641–648.
4. Serneri GG, Modesti PA, Boddi M, Cecioni I, Galanti G, Papa L, Bandinelli B, Maccherini M, Sani G, Toscano M. Cardiac growth factors in human hypertrophy. Relations with myocardial contractility and wall stress. *Circ Res.* 1999;85:57–67.
5. Shioi T, McMullen JR, Kang PM, Franke TF, Cantley LC, Izumo S. Akt/protein kinase B promotes organ growth in transgenic mice. *Mol Cell Biol.* 2002;22:2799–2809.
6. Condorelli G, Drusco A, Stassi G, Bellacosa A, Roncarati R, Gu Y, Dalton N, Napoli C, Sadoshima J, Croce CM, Ross J Jr. Akt induces enhanced myocardial contractility and cell size in vivo in transgenic mice. *Proc Natl Acad Sci U S A.* 2002;99:12333–12338.
7. Bueno OF, De Windt LJ, Tymitz KM, Witt SA, Lefer DJ, Peng CF, Kitsis RN, Molkentin JD. The MEK1–ERK1/2 signaling pathway promotes compensated cardiac hypertrophy in transgenic mice. EMBO *J.* 2000;19:6341–6350.
8. Adams JW, Sakata Y, Davis MG, Wang Y, Brown JH, Dorn GW II. Enhanced Galphaq signaling: a common pathway mediates cardiac hypertrophy and apoptotic heart failure. *Proc Natl Acad Sci U S A.* 1998;95:10140–10145.
9. Petrich GB, Wang Y. Stress-activated MAP kinases in cardiac remodeling and heart failure: new insights from transgenic studies. *Trends Cardiovasc Med.* 2004;14:50–55.
10. Molkentin JD. Calcineurin-NFAT signaling regulates the cardiac hypertrophic response in coordination with the MAPKs. *Cardiovasc Res.* 2004;63:467–475.
11. Strle K, Broussard SR, McCusker RH, Shen WH, Johnson RW, Dantzer R, Kelley KW. Proinflammatory cytokine impairment of insulin-like growth factor I-induced protein synthesis in skeletal muscle myoblasts requires ceramide. *Endocrinology.* 2004;145:4592–4602.
12. O'Connor JC, McCusker RH, Strle K, Johnson RW, Dantzer R, Kelley KW. Regulation of IGF-I function by proinflammatory cytokines: at the interface of immunology and endocrinology. *Cell Immunol.* 2008;252:91–110.
13. Hosenpud JD, Campbell SM, Mendelson DJ. Interleukin-1-induced myocardial depression in an isolated beating heart preparation. *J Heart Transplant.* 1989;8:460–464.
14. Shioi T, Matsumori A, Kihara Y Inoko M, Ono K, Iwasaki A, Matsushima K, Sasayama S. Increased expression of interleukin-1β and monocyte chemotactic and activating factor/monocyte chemoattractant protein-1 in the hypertrophied and failing heart with pressure overload. *Circ Res.* 1997;81:664–671.
15. Ono K, Matsumori A, Shioi T, Furukawa Y, Sasayama S. Cytokine gene expression after myocardial infarction in rat hearts: possible implication in left ventricular remodeling. *Circulation* 1998;98:149–156.

16. Thaik CM, Calderone A, Takahashi N, Colucci WS. Interleukin-1 beta modulates the growth and phenotype of neonatal rat cardiac myocytes. *J Clin Invest*. 1995;96:1093–1099.
17. Palmer JN, Hartogensis WE, Patten M, Fortuin FD, Long CS. Interleukin-1 beta induces cardiac myocyte growth but inhibits cardiac fibroblast proliferation in culture. *J Clin Invest*. 1995;95:2555–2564.
18. Nishikawa K, Yoshida M, Kusuhara M, Isoda K, Miyazaki K, Ohsuzu F. Left ventricular hypertrophy in mice with a cardiac-specific overexpression of interleukin-1. *Am J Physiol Heart Circ Physiol*. 2006;291: H176–H183.
19. Seko Y, Takahashi N, Shibuya M, Yazaki Y. Pulsatile stretch stimulates vascular endothelial growth factor (VEGF) secretion by cultured rat cardiac myocytes. *Biochem Biophys Res Commun*. 1999;254:462–465.
20. Avontuur JAM, Stam TC, Jongen-Lavrencic M, van Amsterdam JGC, Eggermont AMM, Bruining HA. Effect of L-NAME, an inhibitor of nitric oxide synthesis, on plasma levels of IL-6, IL-8, TNFa and nitrite/nitrate in human septic shock. *Intensive Care Med*. 1998;24:673–679.
21. Mata-Greenwood E, Grobe A, Kumar S, Noskina Y, Black SM. Cyclic stretch increases VEGF expression in pulmonary arterial smooth muscle cells via TGF-beta1 and reactive oxygen species: a requirement for NAD(P)H oxidase. *Am J Physiol Lung Cell Mol Physiol*. 2005;289: L288–L289.
22. Siwik AD, Tzortzis DJ, Pimental RD, Chang LFD, Singh K, Sawyer BD, Colucci SW. Inhibition of copper-zinc superoxide dismutase induces cell growth, hypertrophic phenotype, and apoptosis in neonatal rat cardiac myocytes in vitro. *Circ Res*. 1999;85:147–153.
23. Woelfle J, Rotwein P. In vivo regulation of growth hormone-stimulated gene transcription by STAT5b. *Am J Physiol Endocrinol Metab*. 2004; 286:393–401.
24. Wynes WM, Riches WHD. Transcription of macrophage IGF-I exon 1 is positively regulated by the 5′-untranslated region and negatively regulated by the 5′-flanking region. *Am J Physiol Lung Cell Mol Physiol* 2005;288:L1089–L1098.
25. Chia DJ, Ono M, Woelfle J, Schlesinger-Massart M, Jiang H, Rotwein P. Characterization of distinct Stat5b binding sites that mediate growth hormone-stimulated IGF-I gene transcription. *J Biol Chem*. 2006;281: 3190–3197.
26. Werwers MD, Herzyk DJ. Alveolar macrophages differ from blood monocytes in human IL-1β release. *J Immunol*. 1989;143:1635–1641.
27. Davey HW, Xie T, McLachlan MJ, Wilkins RJ, Waxman DJ, Grattan DR. STAT5b is required for GH-induced liver IGF-I gene expression. *Endocrinology*. 2001;142:3836–3841.
28. Manning AM, Davis RJ. Targeting JNK for therapeutic benefit: from junk to gold? *Nat Rev Drug Discov*. 2003;2:554–565.
29. Kamata H, Honda S, Maeda S, Chang L, Hirata H, Karin M. Reactive oxygen species promote TNFalpha-induced death and sustained JNK activation by inhibiting MAP kinase phosphatases. *Cell*. 2005;120: 649–661.
30. Galvan V, Logvinova A, Sperandio S, Ichijo H, Bredesen DE. Type 1 insulin-like growth factor receptor (IGF-IR) signaling inhibits apoptosis signal-regulating kinase 1 (ASK1). *J Biol Chem*. 2003;278:13325–13332.
31. Takeuchi H, Kim J, Fujimoto A, Umetani N, Mori T, Bilchik A, Turner R, Tran A, Kuo C, Hoon DS. X-linked inhibitor of apoptosis protein expression level in colorectal cancer is regulated by hepatocyte growth factor/C-met pathway via Akt signaling. *Clin Cancer Res*. 2005;11: 7621–7628.
32. Suzuki Y, Nakabayashi Y, Takahashi R. Ubiquitin-protein ligase activity of X-linked inhibitor of apoptosis protein promotes proteasomal degradation of caspase-3 and enhances its anti-apoptotic effect in Fas-induced cell death. *Proc Natl Acad Sci U S A*. 2001;98:8662–8667.
33. Wang L, Ma W, Markovich R, Chen JW, Wang PH. Regulation of cardiomyocyte apoptotic signaling by insulin-like growth factor I. *Circ Res*. 1998;83:516–522.

Identification of ARIA regulating endothelial apoptosis and angiogenesis by modulating proteasomal degradation of cIAP-1 and cIAP-2

Koji Ikeda[a,1], Ritsuko Nakano[a], Maki Uraoka[a], Yusuke Nakagawa[a], Masahiro Koide[a], Asako Katsume[a], Keizo Minamino[b], Eri Yamada[b], Haruhiko Yamada[b], Thomas Quertermous[c], and Hiroaki Matsubara[a,1]

[a]Department of Cardiovascular Medicine, Kyoto Prefectural University School of Medicine, 465 Kajii, Kawaramachi-Hirokoji, Kamigyo, Kyoto 602-8566, Japan; [c]Division of Cardiovascular Medicine, Stanford University, 300 Pasteur Drive, Stanford, CA 94305; and [b]Department of Ophthalmology, Kansai Medical University, 2-3-1 Shinmachi, Hirakata, Osaka573-1191, Japan

Edited by Napoleone Ferrara, Genentech, Inc., South San Francisco, CA, and approved March 20, 2009 (received for review July 14, 2008)

Endothelial apoptosis is a pivotal process for angiogenesis during embryogenesis as well as postnatal life. By using a retrovirus-mediated signal sequence trap method, we identified a previously undescribed gene, termed ARIA (apoptosis regulator through modulating IAP expression), which regulates endothelial apoptosis and angiogenesis. ARIA was expressed in blood vessels during mouse embryogenesis, as well as in endothelial cells both in vitro and in vivo. ARIA is a unique protein with no homology to previously reported conserved domain structures. Knockdown of ARIA in HUVECs by using small interfering RNA significantly reduced endothelial apoptosis without affecting either cell migration or proliferation. ARIA knockdown significantly increased inhibitor of apoptosis (cIAP)-1 and cIAP-2 protein expression, although their mRNA expression was not changed. Simultaneous knockdown of cIAP-1 and cIAP-2 abolished the antiapoptotic effect of ARIA knockdown. Using yeast 2-hybrid screening, we identified the interaction of ARIA with 20S proteasome subunit α-7. Thereafter, we found that cIAP-1 and cIAP-2 were degraded by proteasomes in endothelial cells under normal condition. Overexpression of ARIA significantly reduced cIAP-1 expression, and this reduction was abolished by proteasomal inhibition in BAECs. Also, knockdown of ARIA demonstrated an effect similar to proteasomal inhibition with respect to not only expression but also subcellular localization of cIAP-1 and cIAP-2. In vivo angiogenesis studied by Matrigel-plug assay, mouse ischemic retinopathy model, and tumor xenograft model was significantly enhanced by ARIA knockdown. Together, our data indicate that ARIA is a unique factor regulating endothelial apoptosis, as well as angiogenesis, presumably through modulating proteasomal degradation of cIAP-1 and cIAP-2 in endothelial cells.

Angiogenesis is the process of forming new blood vessels through sprouting and budding of new capillaries from existing blood vessels. Endothelial cells constitute the inner layer of blood vessels and have critical roles in angiogenesis under both physiological and pathological conditions. Because of the central role of angiogenesis in ischemic cardiovascular diseases, as well as in cancer, modulating this process is a promising approach to treat these diseases. In fact, enhancing angiogenesis by administration of growth factors or cell transplantation to treat ischemic diseases and reducing angiogenesis by inhibiting VEGF to treat cancer have been clinically used and demonstrated considerably beneficial effects (1–4). However, use of these therapies is not yet satisfactory, and improvement is certainly needed. To develop better therapeutic angiogenesis, it is crucial to understand its detailed molecular mechanism, including unknown factors regulating endothelial cell function.

Membrane proteins, as well as secreted proteins expressed in endothelial cells, are known to have specific and critical roles in the regulation of endothelial function and angiogenesis (5–7). To identify novel factors regulating endothelial function and angiogenesis, we performed a signal sequence trap screening that specifically traps genes encoding secreted and membrane proteins. Here, we characterize a previously undescribed gene, named ARIA (apoptosis regulator through modulating IAP expression). ARIA is expressed in endothelial cells both in vitro and in vivo, as well as in blood vessels, during mouse embryogenesis. Knockdown of ARIA expression in human umbilical vein endothelial cells (HUVECs) significantly reduced apoptosis by increasing inhibitor of apoptosis (cIAP)-1 and cIAP-2 protein expression. In vitro and in vivo studies indicate a significant role for this factor in angiogenesis.

Results

Isolation of ARIA. To isolate novel factors regulating endothelial cell function and angiogenesis, we have employed a signal sequence trap using a cDNA library prepared from human microvascular endothelial cells. One gene we have isolated demonstrated significant expression in endothelial cells, whereas no expression was observed in nonendothelial cells (Fig. 1*A*). We named this gene ARIA and further analyzed its function in endothelial cells. ARIA was also expressed in vascular smooth muscle cells, as well as in hematopoietic cells such as macrophages, lymphocytes, and mast cells, although those expression levels appeared to be much lower than in endothelial cells (Fig. 1 *B* and *C*). In adult mouse tissues, ARIA was expressed in all tissues examined, and the highest expression was observed in lung and spleen (Fig. 1 *D* and *E*). In situ hybridization of ARIA in embryonic day 9.5 (e9.5d) mouse embryo demonstrated its expression in blood vessels (Fig. 2*A* and *B*). ARIA was expressed as early as e7.5d, and its expression was maintained at least until e15.5d (Fig. 2*C*). These results suggest that ARIA might be a previously undescribed factor regulating endothelial cell function and angiogenesis.

Expression of ARIA in Vitro and in Vivo. Full-length human and mouse ARIA cDNAs were isolated as described in *Materials and Methods*. The sequences of these genes have been submitted to the GenBank database under accession nos. EU025066 (human ARIA) and EU025067 (mouse ARIA). The amino acid sequences of both human and mouse ARIA contained a putative transmembrane domain (Fig. 3*A*). Overall amino acid sequence homology between human and mouse ARIA was ≈61%. However, when focusing on

Author contributions: K.I., H.Y., T.Q., and H.M. designed research; K.I., R.N., M.U., Y.N., M.K., A.K., K.M., E.Y., and H.Y. performed research; K.I. and H.Y. analyzed data; and K.I., T.Q., and H.M. wrote the paper.

The authors declare no conflict of interest.

This article is a PNAS Direct Submission.

Freely available online through the PNAS open access option.

Data deposition: The sequences reported in this paper have been deposited in the GenBank database [accession nos. EU025066 (human ARIA) and EU025067 (mouse ARIA)].

[1]To whom correspondence may be addressed. E-mail: ikedak@koto.kpu-m.ac.jp or matsubah@koto.kpu-m.ac.jp.

This article contains supporting information online at www.pnas.org/cgi/content/full/0806780106/DCSupplemental.

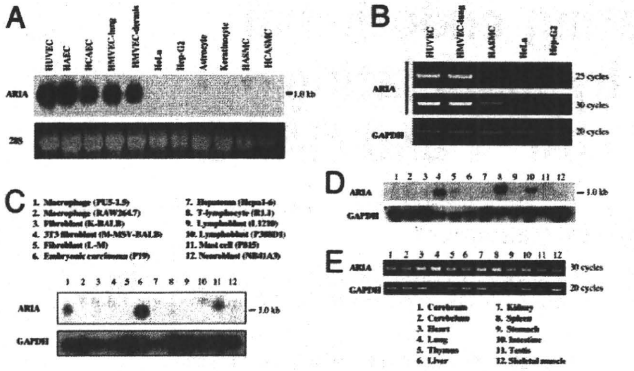

Fig. 1. Messenger RNA expression of ARIA. (*A*) Northern blot analysis of ARIA in primary cultured human endothelial cells and other cultured human cells. Cells examined were HUVEC, human aortic endothelial cells (HAEC), human coronary artery endothelial cells (HCAEC), human lung microvascular endothelial cells (HMVEC-lung), human dermal microvascular endothelial cells (HMVEC-dermis), HeLa, human hepatoma cells (Hep-G2), human astrocytes, human keratinocytes, human aortic smooth muscle cells (HASMC), and human coronary artery smooth muscle cells (HCASMC). (*B*) RT-PCR analysis of ARIA. Little expression of ARIA was observed in vascular smooth muscle cells, but not in HeLa or Hep-G2 cells. (*C*) Northern blot analysis of ARIA in mouse cell line MTN blot (BD Clontech). ARIA was expressed in some of hematopoietic cells. (*D*) Northern blot analysis of ARIA in mouse tissues. (*E*) RT-PCR analysis of ARIA in mouse tissues.

the C-terminal region, including the putative transmembrane domain, their homology was ≈91%, suggesting that this region may have an important role in ARIA function. When expressed in HeLa cells, recombinant proteins tagged with FLAG of both human and mouse ARIA migrated at ≈60 kDa, which is significantly larger than the predicted molecular mass (≈24 kDa), suggesting that

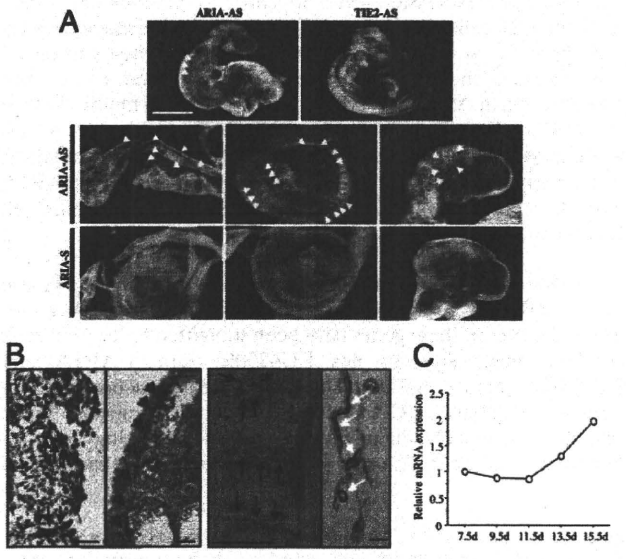

Fig. 2. Expression of ARIA during mouse embryogenesis. (*A*) Whole-mount in situ hybridization of ARIA in e9.5d mouse embryo. ARIA was expressed in blood vessels during embryogenesis as indicated by arrows (ARIA-AS). Negative control using sense cRNA probe (ARIA-S) did not show significant signals. In situ hybridization of TIE-2, expressed almost exclusively in endothelial cells and early hematopoietic cells, was performed for a positive control of the blood vessel expression. (*B*) Sections of embryo from the whole-mount in situ hybridization. ARIA expression was observed in intersomitic arteries, dorsal aorta (black arrows), and blood vessels on the yolk sac (white arrows). (Scale bars, 100 μm.) (*C*) Relative expression of ARIA in the whole embryos at indicated embryonic day.

ARIA undergoes posttranslational modification (Fig. 3*B*). We generated anti-mouse ARIA antibody by using a mixture of 3 epitopes of mouse ARIA. This antibody successfully detected endogenous ARIA in mouse endothelial cells (py4.1), but did not cross-react well with human ARIA, and failed to detect it in HUVECs (Fig. 3*B*). Immunocytochemistry using anti-FLAG antibody demonstrated that human ARIA was expressed in cytosol, as well as on plasma membrane (Fig. 3*C*). A FLAG epitope tag was added at the C terminus for the detection of recombinant protein. Because no signal was observed without permeabilization treatment with Triton X-100, the C terminus of membrane-bound ARIA is likely located in the intracellular region (Fig. 3*C*). Endogenous mouse ARIA detected by the anti-ARIA antibody was also localized both in cytosol and on plasma membrane in py4.1 mouse endothelial cells (Fig. 3*C*).

Immunohistochemistry of ARIA in mouse lung and spleen demonstrated its expression in endothelial cells, as well as in vascular smooth muscle cells, bronchial epithelial cells, a subset of lymphocytes, and macrophages (Fig. 3*D*). These in vivo expression profiles of ARIA were consistent with the in vitro expression analysis.

ARIA Regulates Endothelial Apoptosis. To investigate ARIA function in endothelial cells, we prepared 2 independent siRNAs to knock down ARIA expression. Negative control siRNA (scramble siRNA) was used as a control. We have confirmed effective transfection of siRNA in HUVECs by electroporation, as well as by using RNAiMAX reagent (Fig. S1*A*). Both ARIA siRNAs (KD1 and KD2) effectively knocked down ARIA mRNA expression in HUVECs by electroporation (Fig. 4*A*) and by using RNAiMAX reagent (Fig. S1*B*). When apoptosis was induced by serum and growth factor depletion, ARIA knockdown resulted in significant reduction of endothelial apoptosis as compared with cells transfected with the scramble siRNA (Fig. 4*B*). In contrast, ARIA knockdown did not affect either endothelial cell migration or proliferation (Fig. S2), suggesting that ARIA is closely involved in the regulation of endothelial apoptosis.

Also, analysis of the expressional regulation of ARIA revealed that some cytokines such as TNF-α and TGF-β decreased ARIA expression in endothelial cells (Fig. S3).

ARIA Regulates Endothelial Apoptosis by Modulating cIAP-1 and cIAP-2 Expression. To elucidate the molecular mechanism responsible for the antiapoptotic effect of ARIA knockdown, signals and molecules regulating cell apoptosis were analyzed by immunoblotting. Phosphorylation of MAPK families, as well as Akt, was not affected by ARIA knockdown (Fig. S4*A*). We also observed that reactive oxygen species production assessed by dichlorodihydrofluorescein (DCF) fluorescence was not affected by the ARIA knockdown (Fig. S4*B*). Finally, we identified that cIAP-1 (Birc2) and cIAP-2 (Birc3) protein expression was significantly increased in HUVECs as a result of ARIA knockdown (Fig. 4*C*). In contrast, X-linked IAP (XIAP) was not increased by ARIA knockdown (Fig. 4*C*). Simultaneous knockdown of cIAP-1 and cIAP-2 abrogated the antiapoptotic effect of ARIA knockdown (Fig. 4*D*). Knockdown of cIAP-1 and cIAP-2 was confirmed at the protein level, as well as at the mRNA level (Fig. S5). These results indicate that ARIA regulates endothelial cell survival through modulating cIAP-1 and cIAP-2 expression.

Despite their increased protein expression, mRNA level of both cIAP-1 and cIAP-2 was not increased by ARIA knockdown (Fig. S5*C*). These results suggest that ARIA probably modulates cIAP-1 and cIAP-2 expression at the protein level in endothelial cells.

ARIA Modulates Proteasomal Degradation of cIAP-1 and cIAP-2. To identify the binding partner of ARIA in HUVECs, we have performed yeast 2-hybrid screening using the highly conserved C-terminal region of human ARIA as bait. One positive clone

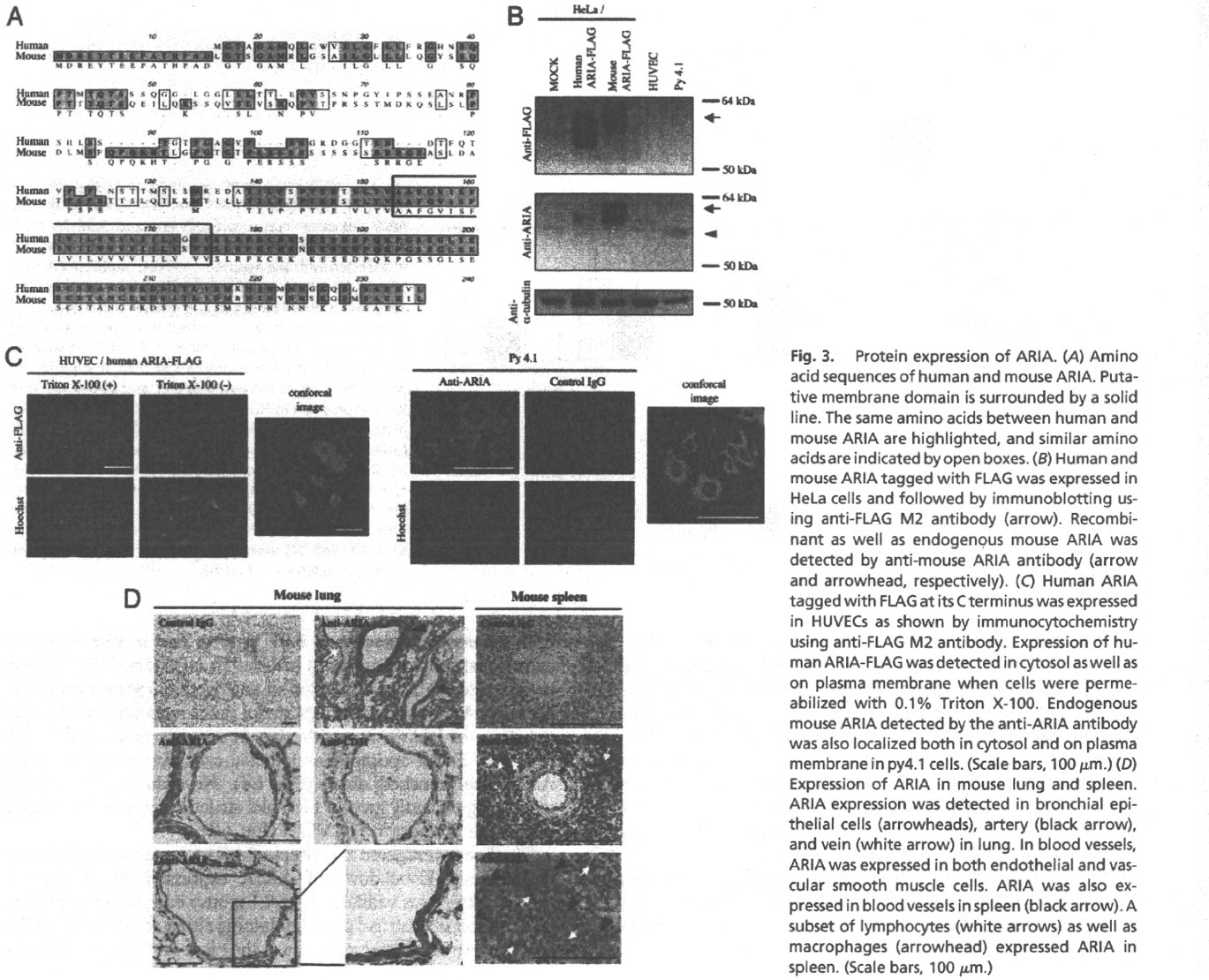

Fig. 3. Protein expression of ARIA. (*A*) Amino acid sequences of human and mouse ARIA. Putative membrane domain is surrounded by a solid line. The same amino acids between human and mouse ARIA are highlighted, and similar amino acids are indicated by open boxes. (*B*) Human and mouse ARIA tagged with FLAG was expressed in HeLa cells and followed by immunoblotting using anti-FLAG M2 antibody (arrow). Recombinant as well as endogenous mouse ARIA was detected by anti-mouse ARIA antibody (arrow and arrowhead, respectively). (*C*) Human ARIA tagged with FLAG at its C terminus was expressed in HUVECs as shown by immunocytochemistry using anti-FLAG M2 antibody. Expression of human ARIA-FLAG was detected in cytosol as well as on plasma membrane when cells were permeabilized with 0.1% Triton X-100. Endogenous mouse ARIA detected by the anti-ARIA antibody was also localized both in cytosol and on plasma membrane in py4.1 cells. (Scale bars, 100 μm.) (*D*) Expression of ARIA in mouse lung and spleen. ARIA expression was detected in bronchial epithelial cells (arrowheads), artery (black arrow), and vein (white arrow) in lung. In blood vessels, ARIA was expressed in both endothelial and vascular smooth muscle cells. ARIA was also expressed in blood vessels in spleen (black arrow). A subset of lymphocytes (white arrows) as well as macrophages (arrowhead) expressed ARIA in spleen. (Scale bars, 100 μm.)

encodes 70 aa of C-terminal region of 20S proteasome subunit α (PSMA)-7. PSMA-7 is one of the subunits constituting cylinder-shaped 20S core proteasome and is located at the outer rings flanking an internal pair of β rings (8). We confirmed their interaction by coprecipitation of HA-tagged PSMA-7 and FLAG-tagged ARIA expressed in bovine aortic endothelial cells (BAECs) (Fig. 5*A*).

Although it has been reported that IAPs undergo proteasomal degradation on apoptotic stimuli in thymocytes (9), it is unclear whether they are also degraded by proteasomes in endothelial cells, especially under normal conditions. Interaction of ARIA with the proteasome subunit urged us to investigate its function in the proteasomal degradation of cIAP-1 and cIAP-2. We first explored whether cIAP-1 and cIAP-2 are degraded by proteasomes in endothelial cells under normal conditions. Inhibition of proteasomes by MG132 significantly increased cIAP-1 and cIAP-2, but not XIAP, expression in HUVECs, indicating that cIAP-1 and cIAP-2 are indeed degraded by proteasomes in endothelial cells under normal conditions (Fig. 5*B*).

In contrast, treatment with MG132 failed to further increase cIAP-1 and cIAP-2 expression in HUVECs when ARIA was knocked down (Fig. 5*C*). These results suggest that proteasomal degradation of cIAP-1 and cIAP-2 was reduced by ARIA knockdown. Also, overexpression of ARIA significantly reduced cIAP-1 expression in BAECs (Fig. 5*D*). Notably, this effect of ARIA overexpression was abolished by proteasome inhibition, indicating that ARIA positively regulates the proteasomal degradation of cIAP-1 in endothelial cells (Fig. 5*D*). Because our antibody did not recognize bovine cIAP-2, we could not assess cIAP-2 expression in BAECs.

We then investigated expression and subcellular localization of cIAP-1, cIAP-2, and XIAP in HUVECs by immunocytochemistry. Interestingly, they demonstrated distinct subcellular localization; cIAP-1 was in cytosol, cIAP-2 was largely in nucleus, and XIAP was in both cytosol and nucleus in the control HUVECs (Fig. 5*E*). When proteasomal degradation was inhibited by MG132, cIAP-1 accumulated in the perinuclear region with the appearance of small structures, whereas cytosolic expression of cIAP-2 was evenly enhanced (Fig. 5*E*). Expression and subcellular localization of XIAP were not significantly affected by MG132 treatment. Of note, expression, as well as subcellular localization of cIAP-1 and cIAP-2 in ARIA-knocked-down HUVECs were very similar to those in the control cells treated with MG132 (Fig. 5*E*).

To examine whether ARIA is involved in the proteasomal degradation specifically for cIAP-1 and cIAP-2, we investigated the effect of ARIA knockdown on the expression of other proteins